



---

# Applied Computational Electromagnetics Society

---



**Newsletter**  
**Volume 17 - No. 3**  
**ISSN 1056-9170**



November 2002



# **APPLIED COMPUTATIONAL ELECTROMAGNETICS SOCIETY (ACES)**

## **NEWSLETTER**

Vol. 17 No. 3

November 2002

### **TABLE OF CONTENTS**

#### **OFFICERS' REPORTS**

President's Post- Osama A. Mohammed ..... 4

#### **COMMITTEE REPORTS**

ACES Committees ..... 5

Publications Committee - Andrew Peterson ..... 6

Elections Report - Rene J. Allard ..... 7

#### **TECHNICAL FEATURE ARTICLE - "Simulation of Nonuniform High-Speed Interconnects with Frequency Dependent Parameters by Wavelets on the Interval"**

S. Barmada and M. Raugi ..... 8

#### **TUTORIAL ARTICLE - "Fast Multipole Formulation for PEEC Frequency Domain Modeling"**

Giulio Antonini ..... 22

#### **PERSPECTIVES IN CEM - "Application of some Common Numerical Methods to Simple Radiation and Scattering Problems"- David Jenn and Yeo Chee Beng.....**

39

#### **SOFTWARE REPORT - Two-Dimensional TM and TE FDTD Codes with Visualization"**

Allen Glisson, Atef Elsherbeni, and Chun-Wen P. Huang ..... 51

#### **ANNOUNCEMENTS:**

APPLICATION for ACES Membership, Newsletter and Journal Subscription ..... 66

ADVERTISING Rates ..... 67

DEADLINE for Submission of Articles ..... 67

## ACES NEWSLETTER STAFF

### EDITOR-IN-CHIEF, NEWSLETTER

Bruce Archambeault  
IBM  
3039 Cornwallis Road, PO Box 12195  
Dept. 18DA B306  
Research Triangle Park, NC 27709  
Phone: 919-486-0120  
email:barch@us.ibm.com

### ASSOCIATE EDITOR-IN-CHIEF

Ray Perez  
Martin Marietta Astronautics  
MS 58700, PO Box 179  
Denver, CO 80201, U.S.A  
Phone: 303-977-5845  
Fax: 303-971-4306  
email:ray.j.perez@lmco.com

### EDITOR-IN-CHIEF, PUBLICATIONS

Andrew Peterson  
Georgia Institute of Technology, ECE  
777 Atlantic Drive  
Atlanta, GA 30332-0250  
Phone: 404-894-4697  
Fax: 404-904-5935  
email:peter@ee.gatech.edu

### MANAGING EDITOR

Richard W. Adler  
Pat Adler, Production Assistant  
Naval Postgraduate School/ECE Department  
Code ECAB, 833 Dyer Road, Room 437  
Monterey, CA 93943-5121, U.S.A.  
Phone: 831-646-1111  
Fax: 831-649-0300  
email:rwa@attglobal.net

## EDITORS

### CEM NEWS FROM EUROPE

Pat R. Foster  
Microwaves and Antenna Systems  
16 Peachfield Road  
Great Malvern, Worc, UK WR14 4AP  
Phone: +44 1684 5744057  
Fax: +44 1684 573509  
email:prf@maasdesign.co.uk

### MODELER'S NOTES

Gerald Burke  
Lawrence Livermore National Labs.  
Box 5504/L-156  
Livermore, CA 94550, U.S.A.  
Phone: (510) 422-8414  
Fax: (510) 422-3013  
email:burke2@llnl.gov

### TECHNICAL FEATURE ARTICLE

Andy Drozd  
ANDRO Consulting Services  
PO Box 543  
Rome, NY 13442-0543 U.S.A.  
phone: (315) 337-4396  
Fax: (314) 337-4396  
email:andro1@aol.com

### PERSPECTIVES IN CEM

Manos M. Tentzeris  
Georgia Institute of Technology  
ECE Dept.  
Atlanta, GA 30332-0250  
Phone: (404) 385-0378  
email:eentze@ece.gatech.edu

### THE PRACTICAL CEMIST

W. Perry Wheless, Jr.  
University of Alabama  
P.O. Box 11134  
Tuscaloosa, AL 35486-3008, U.S.A.  
Phone: (205) 348-1757  
Fax: (205) 348-6959  
email:wwheless@ua1vm.ua.edu

### TUTORIAL

J. Alan Roden  
IBM Microelectronics  
Dept. OSXA  
3039 Cornwallis Road  
Research Triangle Park, NC 27709  
Phone: (919) 543-8645  
email:jaroden@us.ibm.com

## ACES JOURNAL

### EDITOR-IN-CHIEF

Atef Elsherbini  
EE Department, Anderson Hall  
University of Mississippi  
University, MS 38677-U.S.A.  
Phone (662) 915-5382  
email:atef@olemiss.edu

## **NEWSLETTER ARTICLES AND VOLUNTEERS WELCOME**

The ACES Newsletter is always looking for articles, letters, and short communications of interest to ACES members. All individuals are encouraged to write, suggest, or solicit articles either on a one-time or continuing basis. Please contact a Newsletter Editor.

## **AUTHORSHIP AND BERNE COPYRIGHT CONVENTION**

The opinions, statements and facts contained in this Newsletter are solely the opinions of the authors and/or sources identified with each article. Articles with no author can be attributed to the editors or to the committee head in the case of committee reports. The United States recently became part of the Berne Copyright Convention. Under the Berne Convention, the copyright for an article in this newsletter is legally held by the author(s) of the article since no explicit copyright notice appears in the newsletter.

### **BOARD OF DIRECTORS**

### **EXECUTIVE COMMITTEE**

Osama Mohammed, President	Allen W. Glisson, Treasurer
Bruce Archambeault, Vice President	Richard W. Adler, Executive Officer
Keith Lysiak, Secretary	

### **DIRECTORS-AT-LARGE**

Masanori Koshiba	2003	Bruce Archambeault	2004	Allen W. Glisson	2005
Osama Mohammed	2003	Andrzej Krawczyk	2004	Keith Lysiak	2005
Tapan Sarkar	2003	Ray Perez	2004	Eric Mechielssen	2005

### **ACES ELECTRONIC PUBLISHING GROUP**

<b>Atef Elsherbeni</b>	<b>Electronic Publication Managing Editor</b>
<b>Matthew J. Inman</b>	<b>Site Administrator</b>
<b>Jessica Drewrey</b>	<b>Assistant Administrator</b>
<b>Brad Baker</b>	<b>Contributing Staff</b>
<b>Imran Kader</b>	<b>Past Administrator</b>
<b>Chris Riley</b>	<b>Past Staff</b>

Visit us on line at:  
<http://aces.ee.olemiss.edu>

## **PRESIDENT'S POST**

Preparations for the ACES annual conference are in full swing. It will be held March 24-28, 2003. The conference is our society's main event and its continued success is everyone's business. We look forward to the support of everyone who can help make the 2003 conference in Monterey, CA a great event. The ACES annual conference is a highly influential outlet for promoting awareness of recent technical contributions to the advancement of computational electromagnetics. Attendance of ACES members as well as nonmembers from throughout the world is encouraged and welcomed. The Board of Directors invites every ACES member to participate and encourage their colleagues to submit and present papers at the annual conference and/or organize a session, tutorial or participate in the vendor exhibit.

This year's conference will feature few changes from previous years. These changes are meant to enhance interaction among research groups around the world and increase industrial, academic and government agency participation. The conference will feature plenary and panel sessions, where invited speakers deliver original essay-like reviews of hot topics of interest to the computational electromagnetics community. It will also feature oral-invited sessions, poster sessions, a student paper competition, short courses (full-day and half-day), and vendor exhibits, which will feature several companies exhibiting their products. A cash prize will be awarded to the authors of the best non-student paper presented (poster or oral) at the conference and the judging will be performed a special ACES prize-paper committee. The conference will also include several social events including the annual awards banquet. The welcome reception will be organized in the evening of Sunday March 23, 2003 where we can all gather and kick off the conference.

Another new feature of the 2003 conference is that all authors of accepted papers will have the option to submit an extended version of their paper or papers for review and publication in special issues of the ACES Journal.

Awards represent an important activity of our society. Several awards will be given to several of our colleagues at the conference's awards banquet. Please submit your nominations to the society's awards chair, Pat Foster for the various awards. These awards include; valued service award, exemplary service award, founders award, mainstay award and outstanding paper award. More information about the society's awards program can be found on the ACES website. We are also looking for several ACES members to serve on committees to increase the leadership pool and help the society serve its members. If you are interested, let me know by phone, fax or e-mail.

In an effort to increase membership service, conference proceedings and journal archives are available on CD for ACES members and nonmembers. The ACES website includes information on how to obtain your copies of these archives. Increasing membership and services as well as enhancing the attendance at the conference are important goals to maintaining the viability of our society. As president, I will continue to promote ACES on all fronts. The BoD invites all members to participate in achieving these goals.

O. A. Mohammed  
President, ACES

**PERMANENT STANDING COMMITTEES OF ACES INC.**

<b>COMMITTEE</b>	<b>CHAIRMAN</b>	<b>ADDRESS</b>
NOMINATIONS	Rene Allard	Penn State University PO Box 30 State College, PA 16804-0030
ELECTIONS	Rene Allard	Penn State University PO Box 30 State College, PA 16804-0030
FINANCE	Allen Glisson	EE Department, Anderson Hall University of Mississippi University, MS 38677
PUBLICATIONS	Andrew Peterson	Georgia Institute of Technology School of ECE Atlanta, GA 30332-0250
CONFERENCE	Osama Mohammed	Florida International University ECE Department Miami, FL 33174
AWARDS	Pat Foster	MAAS 16 Peachfield Road Great Malvern, UK WR14 4AP

**MEMBERSHIP ACTIVITY COMMITTEES OF ACES INC.**

<b>COMMITTEE</b>	<b>CHAIRMAN</b>	<b>ADDRESS</b>
SOFTWARE VALIDATION	Bruce Archambeault	IBM 158 Lin Tilley Road Durham, NC 27712
HISTORICAL	Robert Bevensee	BOMA Enterprises PO Box 812 Alamo, CA 94507-0812

## **PUBLICATIONS COMMITTEE REPORT**

I am pleased to report that in July 2002, ACES made a formal request to the Institute for Scientific Information (ISI) asking that the ACS Journal be included in the ISI database. The ISI database provides an index to about 8600 international journals, including bibliographic data and reference citations. This request was made in part because of a number of member requests that we do so. Inclusion in the ISI database should help the outside world locate relevant articles in the Journal and raise the visibility of the Journal.

The evaluation process may take some time, since the ISI editors require that several issues be sent to them as they appear (in order to judge the frequency of publication and the adherence to the indicated schedule). We are optimistic that we will receive a positive response from them sometime next year!

Professor Andrew F. Peterson  
School of Electrical & Computer Engineering  
Georgia Institute of Technology  
Atlanta, GA 30332-0250  
USA

(404)-894-4697 (office)  
(770)-454-9557 (home)  
(404)-894-4641 (shared department FAX)  
peterson@ee.gatech.edu

## **ELECTION REPORT**

Candidate statements appeared in the July ACES Newsletter.

Congratulations go to Leo Kemple, Tapan Sarkar and Osama Mohammed.

These three newly elected Directors will be installed in office at the next Annual Meeting of Members which occurs at the annual conference.

Rene Allard, Elections Committee Chairman



# Simulation of Nonuniform High-speed Interconnects with Frequency Dependent Parameters by Wavelets on the Interval

S. Barmada, M. Raugi

Dipartimento di Sistemi Elettrici e Automazione,  
Università di Pisa, via Diotisalvi, 2 56126 Pisa Italy  
Tel: +39 050 565111 Fax: +39 050 565333  
sami.barmada@dsea.unipi.it raugi@dsea.unipi.it

## Abstract

A wavelet approach to the analysis of nonuniform high-speed interconnects with frequency dependent parameters is presented in this paper. The nonuniform interconnects are modeled by the use of nonuniform multiconductor transmission line equations in the frequency domain. Two different methods are proposed here (differential and integral formulation): in both of them the space variable is expanded on a wavelet basis, yielding an algebraic system in the wavelet - frequency domain. The algebraic system is then easily solved by the use of standard techniques; the results are inverse transformed yielding the behavior of voltage and current in the frequency domain. Inverse FFT (Fast Fourier Transform) gives the time domain solution.

## 1 Introduction

The transient analysis of interconnections is a fundamental tool for the synthesis and design of high speed systems such as printed circuit board (PCB) or multichip modules (MCM) in order to determine distortion, crosstalk and other EMC effects that can affect the performances of high density electronics.

A number of numerical techniques [1]-[10] have been reported in the past for the computer simulation of these systems, initially considering uniform lines, and subsequently taking into account nonuniformity and frequency dependent parameters, whose effects cannot be actually neglected in high speed applications.

The Fourier or Laplace transform techniques usually require the inversion of transcendental or hyperbolic functions and in many cases are not efficient; the method of characteristics has been coupled with recursive convolution integral or line discretization along the length and was generalized for skin-effect problems at the cost of an increase of CPU times or memory requirements, furthermore in some cases an accurate evaluation of the impulse response of the line is required. The waveform relaxation is an iterative technique that solves the TL equations in the frequency domain and uses FFT to transform the results back and forth between time and frequency domain at each iteration, but would require too many data points to avoid aliasing effects when very fast signals have to be studied.

Numerical modeling directly in the time domain by differential methods (DM), mainly based on finite elements (FE) and finite-difference time-domain (FDTD), yields a straight modeling of the problem but it is normally coupled with convolution integrals. Furthermore, these methods need dense discretization of the line where the signal is rapidly varying, since the signal propagates along the line the discretization in space should "follow" the signal motion, and this usually leads to the adoption of very fine discretization both in time and space yielding remarkable CPU times.

The wavelet expansion of a function in space characterizes the "harmonic" content of the function at every coordinate, then wavelet basis functions have very good localization properties in space. In particular

the ability of wavelets to focus on short interval for high frequency components and long intervals for low frequency components makes the method effective to represent non-smooth functions since they automatically concentrate in the fast varying regions, and therefore overcoming the DM limitations.

Recently wavelet expansion has been used to solve TL transients [11]. Voltages and currents have been expanded in space by wavelets and a representation of the entire line has been obtained. The final equation is a function of time that is numerically integrated with a standard Runge-Kutta method.

Wavelet expansion has already been used by the authors for the solution of MTL transients [12], [13]; in this paper frequency dependent parameters coupled with nonuniformity have been included. Non-linearities are not included here, but the problem here studied is anyway challenging since there are several applications in which linear loads and frequency dependent parameters are present. Wavelet expansion in space is applied to frequency domain MTL nonuniform equations yielding an algebraic system whose solution, represented by the sample of voltages at the line ports in the frequency domain, is transformed in time domain by FFT. Hence, a numerical solution with no time stepping and iterative procedures has been developed avoiding also the inversion of transcendental functions is obtained. Besides by the use of the WE the system matrices are highly sparse, and by the use of numerical techniques optimized for sparse matrices, very low CPU times can be obtained. Furthermore by thresholding the elements of the matrix [16] it is possible control the sparsity of the system, hence to control the CPU time, while the accuracy of the results are not dramatically affected. This discretization procedure produces systems of algebraic equations which have good condition numbers.

Among the many available wavelet basis in the literature, we choose the compact support Daubechies wavelets and wavelets on the interval. They have the advantage of correctly representing polynomials of degree  $N$  and their regularity increases with  $N$  ( $N$  number of their vanishing moments), more exactly the Holder continuity coefficient increases with  $N$ . A greater regularity leads also to a wider numerical support, then there is a trade-off between the order of the approximation and the numerical cost.

## 2 Wavelets on the Interval and Operators

The concepts of scaling functions, wavelets, time-scale analysis, multiresolution analysis are here considered known [14]; there are many wavelets basis available in the literature, and we chose the Daubechies Wavelets on the interval [15] for their numerical properties. In particular the choice of wavelets that "survive" only on intervals is adopted because we are interested in the solution of boundary value problems. For the compact support wavelet there is an important relation that allows a straight computation of the wavelet coefficients of a generic function: it is possible to obtain the coefficients from the samples of the functions itself according to the relation  $\langle \phi_{J,k}, f \rangle = 2^{J/2} f(2^J k)$ , where  $\phi_{J,k}$  is the scaling function of order  $J, k$  of the adopted wavelet basis. Then, the vector of wavelet coefficients  $G = \mathbf{W}g(t_j)$  representing the wavelet transform of a function  $g(t)$  can be obtained by multiplying a matrix  $\mathbf{W}$  related to the adopted wavelet basis and the time samples  $g(t_j)$  corresponding to  $2^{-m}$  equally spaced points in the interval  $[0, 1]$ . Further details about wavelet numerical computation can be found in [16].

The Wavelet Expansion is used to transform a signal into a vector of coefficients according to the relation

$$f(t) = \mathbf{b}(t)\mathbf{f} \quad (1)$$

where  $\mathbf{b}(t)$  is the wavelet basis and  $\mathbf{f}$  is the vector of coefficients constituting the wavelet expansion of the signal. The notation described in (1) will be used throughout the paper.

Wavelets can also represent operators [17]; in particular an operator in the wavelet domain is represented by a matrix of constant entries. The entries of course depend on the chosen basis and the chosen resolution. A representation of the differential and integral operator for the Daubechies wavelets on the interval has been developed by the authors [12], [13]. The matrices obtained are sparse, as shown in the mentioned papers, and this is important for the numerical characteristic of the obtained method and for the CPU times. Besides in this paper we use also the multiplication by an operator in the wavelet domain, as obtained in [12] and [13]. This allows the representation of nonuniform lines in the wavelet domain when wavelet expansion in space is performed.

## 2.1 Solution of first order differential equations in the wavelet domain

The following is a differential equation and the relative boundary condition:

$$\dot{y} + ay = u \quad y(0) = y_0 \quad (2)$$

By expanding  $y(t)$  and exploiting the definition of operators on a wavelet basis we obtain the system:

$$\begin{cases} \mathbf{D}\mathbf{Y} + a\mathbf{Y} = \mathbf{U} \\ \mathbf{b}_0\mathbf{Y} = y_0 \end{cases} \quad (3)$$

Vectors  $\mathbf{Y}$  and  $\mathbf{U}$  are vectors representing the wavelets coefficients of the unknowns  $y$  and the known terms  $u$  and their dimension is  $2^{-m}$  (with  $m < 0$ ), according to the chosen resolution. The subscript 0 denotes the lower bound value of  $\mathbf{Y}$ ;  $\mathbf{D}$  is the differential operator and has dimension  $2^{-m} \times 2^{-m}$  and the differentiation is performed in the wavelet domain simply by multiplying the matrix by the vector of coefficients representing the quantity to be derived.  $\mathbf{b}_0$  is a constant vector, whose components are the values of the basis functions on the left border of the interval. System (3) can be solved only in the least square sense since it is characterized by  $n + 1$  equations in  $n$  unknown wavelet coefficients. Nevertheless the solution gives accurate result. Qualitatively this fact can be explained because the initial condition has to be known to solve the problem, then the first  $n$  equations cannot represent the actual solution.

Indeed, the matrix  $\mathbf{D} + a\mathbf{I}$  is very ill conditioned, furthermore when  $a = 0$  the differential operator  $\mathbf{D}$  cannot be inverted to obtain the solution because different functions have same derivatives, hence  $\mathbf{D}^{-1}\mathbf{D} \neq \mathbf{I}$ . This means that the information given by equation (2b) is necessary to determine the actual solution and does not yield a redundant boundary on the first  $n$  equation. To get the solution by a  $n \times n$  system of equations the eq. (2b) has been included in the system modifying the operator  $\mathbf{D}$  and the known term as follows:

$$(\mathbf{D} + \mathbf{B}_0)\mathbf{Y} + a\mathbf{Y} = \mathbf{D}'\mathbf{Y} + a\mathbf{Y} = \mathbf{U} + \mathbf{Y}_0 \quad (4)$$

where  $\mathbf{B}_0$  is a matrix with all rows equal to the  $\mathbf{b}_0$  vector and  $\mathbf{Y}_0$  is a vector with all elements equal to  $y_0$ .

## 2.2 Solution of integral equations in the wavelet domain

The following is a general integral equation:

$$y(t) - y(0) + a \int_0^t y(\tau) d\tau = \int_0^t u(\tau) d\tau \quad (5)$$

and its representation in the wavelet domain is:

$$\mathbf{I}_d[\mathbf{Y} - \mathbf{Y}_0] + a\mathbf{T}\mathbf{Y} = \mathbf{T}\mathbf{U} \quad (6)$$

where  $\mathbf{I}_d$  is the identity matrix,  $\mathbf{T}$  is the wavelet representation of the integral operator and the capital letters denote vectors representing the wavelets coefficients of unknowns  $y$  and known terms  $u$ . The initial conditions are taken into account explicitly by the  $\mathbf{Y}_0$  term. The  $\mathbf{Y}$ ,  $\mathbf{Y}_0$ ,  $\mathbf{U}$  are again wavelet coefficients vectors, and their dimension is  $2^{-m}$  (with  $m < 0$ ), according to the chosen resolution. The matrix  $\mathbf{T}$  has dimension  $2^{-m} \times 2^{-m}$  and the integration is performed in the wavelet domain simply by multiplying the matrix by the vector of coefficients representing the quantity to be integrated. The solution is easily obtained by the solution of an algebraic system and it is given by

$$\mathbf{Y} = (\mathbf{I}_d + a\mathbf{T})^{-1}(\mathbf{I}_d\mathbf{Y}_0 + \mathbf{T}\mathbf{U})$$

## 3 Mathematical Formulation

A single conductor nonuniform TL is characterized by the following equations in the frequency domain:

$$\begin{cases} \frac{\partial}{\partial z} \dot{V}(z) = -Z(z, \omega) \dot{I}(z) \\ \frac{\partial}{\partial z} \dot{I}(z) = -Y(z, \omega) \dot{V}(z) \end{cases} \quad (7)$$

where  $Z(z, \omega)$  and  $Y(z, \omega)$  are the per unit length impedance and inductance of the line.

In practical applications it is possible to separate the dependence of  $\omega$  from the dependence from  $z$  (see [18], [19]) hence it is possible to write:

$$Z(z, \omega) = Z_1(z)Z_2(\omega) \quad Y(z, \omega) = Y_1(z)Y_2(\omega) \quad (8)$$

In the following subsections we will obtain the formulations both with the differential and with the integral operator.

### 3.1 Differential formulation

Let us define  $\mathbf{b}(z) = [b_1(z), \dots, b_n(z)]$  as the wavelet basis in the space domain, we can write that

$$\dot{V}(z) = \mathbf{b}(z)\dot{\mathbf{V}} \quad \dot{I}(z) = \mathbf{b}(z)\dot{\mathbf{I}} \quad (9)$$

where  $\dot{\mathbf{V}} = [\dot{V}_1, \dots, \dot{V}_n]^T$  and  $\dot{\mathbf{I}} = [\dot{I}_1, \dots, \dot{I}_n]^T$  are vectors of phasors, i.e. the vectors of coefficients of the wavelet expansion.

Substituting the expansion (9) into (7) we obtain

$$\begin{cases} \frac{\partial}{\partial z} \mathbf{b}(z)\dot{\mathbf{V}} = -Z_2(\omega)\mathbf{b}(z)\mathbf{Z}_1\dot{\mathbf{I}} \\ \frac{\partial}{\partial z} \mathbf{b}(z)\dot{\mathbf{I}} = -Y_2(\omega)\mathbf{b}(z)\mathbf{Y}_1\dot{\mathbf{V}} \end{cases} \quad (10)$$

where  $\mathbf{Z}_1$  and  $\mathbf{Y}_1$  are respectively the matrices of  $Z_1(z)$  and  $Y_1(z)$  obtained as product between functions in the wavelet domain.

By left multiplying by  $\mathbf{b}(z)^T$  and taking into account the definition of the differential operator in the wavelet domain we obtain that

$$\begin{cases} \mathbf{D}_z \dot{\mathbf{V}} = -Z_2(\omega)\mathbf{Z}_1\dot{\mathbf{I}} \\ \mathbf{D}_z \dot{\mathbf{I}} = -Y_2(\omega)\mathbf{Y}_1\dot{\mathbf{V}} \end{cases} \quad (11)$$

where  $\mathbf{D}_z$  is the matrix representing the differential operator in the wavelet domain.

The boundary conditions are given by the equations at the ports of the line; they are respectively

$$\begin{cases} \dot{V}(0) + Z_s \dot{I}(0) = \dot{E} \\ \dot{V}(L) = Z_L \dot{I}(L) \end{cases} \quad (12)$$

where  $Z_s$ ,  $Z_L$  and  $\dot{E}$  are respectively the input and the output impedance, and the input generator phasor at a certain frequency.

In the wavelet domain we have

$$\begin{cases} \dot{V}(0) = \mathbf{b}_0 \dot{\mathbf{V}} & \dot{I}(0) = \mathbf{b}_0 \dot{\mathbf{I}} \\ \dot{V}(L) = \mathbf{b}_L \dot{\mathbf{V}} & \dot{I}(L) = \mathbf{b}_L \dot{\mathbf{I}} \end{cases} \quad (13)$$

where  $\mathbf{b}_0$  and  $\mathbf{b}_L$  are vectors of constant elements being the values of the function of the wavelet basis respectively at the left border and at the right border of the space interval.

Equations (12) can be rewritten as

$$\begin{cases} \mathbf{b}_0 \dot{\mathbf{V}} + Z_s \mathbf{b}_0 \dot{\mathbf{I}} = \dot{E} \\ \mathbf{b}_L \dot{\mathbf{V}} = Z_L \mathbf{b}_L \dot{\mathbf{I}} \end{cases} \quad (14)$$

Taking into account the equations (11) and (14) we can write the following system as shown in (4):

$$\begin{cases} (\mathbf{D}_z + \mathbf{B}_0)\dot{\mathbf{V}} + (Z_2(\omega)\mathbf{Z}_1 + Z_s\mathbf{B}_0)\dot{\mathbf{I}} = \dot{\mathbf{E}} \\ (Y_2(\omega)\mathbf{Y}_1 + \mathbf{B}_0)\dot{\mathbf{V}} + (\mathbf{D}_z - Z_L\mathbf{B}_L)\dot{\mathbf{I}} = 0 \end{cases} \quad (15)$$

where  $\mathbf{B}_0$  and  $\mathbf{B}_L$  are matrices with all rows equal respectively to  $\mathbf{b}_0$  and  $\mathbf{b}_L$ .

The way the boundary conditions are imposed here is due to the fact that the matrices  $\mathbf{B}_0$  and  $\mathbf{B}_L$  are highly sparse (since only  $N$  entries of the vectors  $\mathbf{b}_0$  and  $\mathbf{b}_L$  are different from zero), besides this method doesn't require any further calculation or additional equations to add to the system.

Equations (15) can be rewritten in the following form

$$\begin{vmatrix} \mathbf{D}_z + \mathbf{B}_0 & Z_2(\omega)\mathbf{Z}_1 + Z_s\mathbf{B}_0 \\ Y_2(\omega)\mathbf{Y}_1 + \mathbf{B}_0 & \mathbf{D}_z - Z_L\mathbf{B}_L \end{vmatrix} \begin{vmatrix} \dot{\mathbf{V}} \\ \dot{\mathbf{I}} \end{vmatrix} = \begin{vmatrix} \dot{\mathbf{E}} \\ 0 \end{vmatrix} \quad (16)$$

System (16) is a square system of dimension  $2n \times 2n$ ; its solutions gives the behavior of the unknowns along the line (function of  $z$ ) in the wavelet domain for each frequency. The standard inverse FFT is used to obtain the time domain response.

### 3.2 Integral formulation

In order to include the boundary conditions we integrate (7) respectively between 0 and  $z$ , and between  $z$  and  $L$  obtaining the two following systems

$$\begin{cases} \dot{V}(z) - \dot{V}(0) = -Z_2(\omega) \int_0^z Z_1(z) \dot{I}(z) dz \\ \dot{I}(z) - \dot{I}(0) = -Y_2(\omega) \int_0^z Y_1(z) \dot{V}(z) dz \end{cases} \quad (17)$$

and

$$\begin{cases} \dot{V}(L) - \dot{V}(z) = -Z_2(\omega) \int_z^L Z_1(z) \dot{I}(z) dz \\ \dot{I}(L) - \dot{I}(z) = -Y_2(\omega) \int_z^L Y_1(z) \dot{V}(z) dz \end{cases} \quad (18)$$

Substituting the expansion (9) into (17) and (18) we obtain

$$\begin{cases} \mathbf{b}(z)\dot{\mathbf{V}} - \mathbf{b}(z)\dot{\mathbf{V}}_0 = -Z_2(\omega) \int_0^z \mathbf{b}(z)\mathbf{Z}_1\dot{\mathbf{I}} dz \\ \mathbf{b}(z)\dot{\mathbf{I}} - \mathbf{b}(z)\dot{\mathbf{I}}_0 = -Y_2(\omega) \int_0^z \mathbf{b}(z)\mathbf{Y}_1\dot{\mathbf{V}} dz \end{cases} \quad (19)$$

and

$$\begin{cases} \mathbf{b}(z)\dot{\mathbf{V}}_L - \mathbf{b}(z)\dot{\mathbf{V}} = -Z_2(\omega) \int_z^L \mathbf{b}(z)\mathbf{Z}_1\dot{\mathbf{I}} dz \\ \mathbf{b}(z)\dot{\mathbf{I}}_L - \mathbf{b}(z)\dot{\mathbf{I}} = -Y_2(\omega) \int_z^L \mathbf{b}(z)\mathbf{Y}_1\dot{\mathbf{V}} dz \end{cases} \quad (20)$$

where the quantities  $\dot{\mathbf{V}}_0$ ,  $\dot{\mathbf{V}}_L$ ,  $\dot{\mathbf{I}}_0$  and  $\dot{\mathbf{I}}_L$  are the wavelet transform of  $\dot{V}(0)$ ,  $\dot{V}(L)$ ,  $\dot{I}(0)$ ,  $\dot{I}(L)$ .

Taking into account the definition of the integral operator we obtain for equations (17) and (18)

$$\begin{cases} \dot{\mathbf{V}} - \dot{\mathbf{V}}_0 = -Z_2(\omega)\mathbf{T}_z\mathbf{Z}_1\dot{\mathbf{I}} \\ \dot{\mathbf{I}} - \dot{\mathbf{I}}_0 = -Y_2(\omega)\mathbf{T}_z\mathbf{Y}_1\dot{\mathbf{V}} \end{cases} \quad (21)$$

$$\begin{cases} \dot{\mathbf{V}}_L - \dot{\mathbf{V}} = -Z_2(\omega)\mathbf{T}_z^T\mathbf{Z}_1\dot{\mathbf{I}} \\ \dot{\mathbf{I}}_L - \dot{\mathbf{I}} = -Y_2(\omega)\mathbf{T}_z^T\mathbf{Y}_1\dot{\mathbf{V}} \end{cases} \quad (22)$$

In (21) and (22)  $\mathbf{T}_z$  is the integral operator, which is transposed in (22) because the integration is from  $z$  to  $L$ .

The boundary conditions (12) can be also rewritten in the wavelet domain in the following form:

$$\begin{cases} \dot{\mathbf{V}}_0 + Z_s\dot{\mathbf{I}}_0 = \dot{\mathbf{E}} \\ \dot{\mathbf{V}}_L = Z_L\dot{\mathbf{I}}_L \end{cases} \quad (23)$$

By multiplying the second equation of (21) by  $Z_s$  and the second equation of (22) by  $Z_L$ , adding them and considering the boundary conditions (23) we obtain the following system:

$$\begin{cases} \dot{\mathbf{V}} + Z_s \dot{\mathbf{I}} + Z_2(\omega) \mathbf{T}_z \mathbf{Z}_1 \dot{\mathbf{I}} + Z_s Y_2(\omega) \mathbf{T}_z \mathbf{Y}_1 \dot{\mathbf{V}} = \dot{\mathbf{E}} \\ -\dot{\mathbf{V}} + Z_L \dot{\mathbf{I}} + Z_2(\omega) \mathbf{T}_z^T \mathbf{Z}_1 \dot{\mathbf{I}} - Z_L Y_2(\omega) \mathbf{T}_z^T \mathbf{Y}_1 \dot{\mathbf{V}} = 0 \end{cases} \quad (24)$$

which can be written in a matrix form:

$$\begin{vmatrix} \mathbf{I}_d + Z_s Y_2(\omega) \mathbf{T}_z \mathbf{Y}_1 & Z_2(\omega) \mathbf{T}_z \mathbf{Z}_1 + Z_s \mathbf{I}_d \\ -\mathbf{I}_d - Z_L Y_2(\omega) \mathbf{T}_z^T \mathbf{Y}_1 & Z_2(\omega) \mathbf{T}_z^T \mathbf{Z}_1 + Z_L \mathbf{I}_d \end{vmatrix} \begin{vmatrix} \dot{\mathbf{V}} \\ \dot{\mathbf{I}} \end{vmatrix} = \begin{vmatrix} \dot{\mathbf{E}} \\ 0 \end{vmatrix} \quad (25)$$

where  $\mathbf{I}_d$  is the identity matrix of proper dimension. System (25) is a square system and the solution is obtained directly. This comes from the fact that the boundary conditions are already included in the integral equations.

### 3.3 Generalization for a multiconductor line

In case the line is multiconductor (constituted by  $n+1$  conductors)  $\dot{\mathbf{V}}$  and  $\dot{\mathbf{I}}$  in (7) are vectors composed by the single conductor quantities  $\dot{V}_1, \dots, \dot{V}_p$  and  $\dot{I}_1, \dots, \dot{I}_p$ ; while the line parameters  $Z(z, \omega)$  and  $Y(z, \omega)$  are matrices. Operating as in the previous paragraph, for both the differential and the integral formulation, we obtain again a system in the form of (16) or (25) with the following differences from the single conductor case:

$$\dot{\mathbf{V}} = \begin{vmatrix} \dot{V}_1 \\ \dot{V}_2 \\ \vdots \\ \dot{V}_p \end{vmatrix} \quad \dot{\mathbf{I}} = \begin{vmatrix} \dot{I}_1 \\ \dot{I}_2 \\ \vdots \\ \dot{I}_p \end{vmatrix}$$

where  $\dot{V}_i$  and  $\dot{I}_i$  are vectors of dimension  $n$ .

The operator matrices  $\mathbf{D}_z$  and  $\mathbf{T}_z$  become (only  $\mathbf{D}_z$  is shown)

$$\bar{\mathbf{D}}_z = \begin{vmatrix} \mathbf{D}_z & 0 & 0 & \cdots & 0 \\ 0 & \mathbf{D}_z & 0 & \cdots & 0 \\ \vdots & \vdots & \vdots & \ddots & \vdots \\ 0 & 0 & 0 & \cdots & \mathbf{D}_z \end{vmatrix}$$

and the matrix  $\mathbf{B}_0$  becomes

$$\bar{\mathbf{B}}_0 = \begin{vmatrix} \mathbf{B}_0 & 0 & 0 & \cdots & 0 \\ 0 & \mathbf{B}_0 & 0 & \cdots & 0 \\ \vdots & \vdots & \vdots & \ddots & \vdots \\ 0 & 0 & 0 & \cdots & \mathbf{B}_0 \end{vmatrix}$$

The matrices of the parameters in the wavelet domain become

$$Z_2(\omega) \mathbf{Z}_1 = \begin{vmatrix} (Z_2(\omega) \mathbf{Z}_1)_{11} & (Z_2(\omega) \mathbf{Z}_1)_{12} & \cdots & (Z_2(\omega) \mathbf{Z}_1)_{1p} \\ (Z_2(\omega) \mathbf{Z}_1)_{21} & (Z_2(\omega) \mathbf{Z}_1)_{22} & \cdots & (Z_2(\omega) \mathbf{Z}_1)_{2p} \\ \vdots & \vdots & \ddots & \vdots \\ (Z_2(\omega) \mathbf{Z}_1)_{p1} & (Z_2(\omega) \mathbf{Z}_1)_{p2} & \cdots & (Z_2(\omega) \mathbf{Z}_1)_{pp} \end{vmatrix}$$

where  $(Z_2(\omega) \mathbf{Z}_1)_{i,j}$  are matrices related to each value of the matrix of the impedance. As for the impedances  $Z_L$  and  $Z_s$ , they become matrices as follows

$$\mathbf{Z}_L = \begin{vmatrix} Z_{L11} \mathbf{I}_d & Z_{L12} \mathbf{I}_d & \cdots & Z_{L1p} \mathbf{I}_d \\ Z_{L21} \mathbf{I}_d & Z_{L22} \mathbf{I}_d & \cdots & Z_{L2p} \mathbf{I}_d \\ \vdots & \vdots & \ddots & \vdots \\ Z_{Lp1} \mathbf{I}_d & Z_{Lp2} \mathbf{I}_d & \cdots & Z_{Lpp} \mathbf{I}_d \end{vmatrix}$$

where  $\mathbf{I}_d$  is the identity matrix of dimension  $n \times n$  and the single impedances  $Z_{Lij}$  are determined, for instance, by a nodal analysis at the ports of the Multiconductor Line. As for the input voltages the resulting known term is

$$\dot{\mathbf{E}} = \begin{bmatrix} \dot{\mathbf{E}}_1 \\ \dot{\mathbf{E}}_2 \\ \vdots \\ \dot{\mathbf{E}}_p \end{bmatrix}$$

## 4 Numerical results

The proposed methods have been first validated on a single conductor lossless line closed on its characteristic resistance, then tested on several cases, both with and without frequency dependent parameters, and compared with a standard FD method. Some results are reported here.

As for the CPU times the systems can be solved by standard methods or by methods optimized for sparse matrices. In the latter case, performed here in this paper, in order to obtain high sparsity and good numerical properties the matrices need to be divided into their real and imaginary part, and the systems need to be solved separately. This is because of the large difference in the magnitudes of the real and imaginary parts. With this procedure we are able to obtain CPU times that are proportional to the dimension of the matrix, instead of to the square of it. The integral and the differential approaches proposed here give the same results, in all the simulation we have performed, hence only one of the two methods are reported in the results.

### 4.1 Validation of the methods

In order to verify the validity of the methods, they have been tested on a single conductor lossless line with no input resistance and terminated on its characteristic impedance. Its parameters are respectively

$$l = 28\mu H/m \quad c = 1.2nF/m$$

hence the characteristic impedance is  $R_0 = 152.7525\Omega$ ; the line length is  $0.03m$ .

Figure 1 shows the input and output voltage of the line calculated both by the method proposed here and a standard FD code. It is clearly visible that the signal is transmitted to the end of the line without reflections and with no attenuation. The transit time is also respected. The comparison has been made in

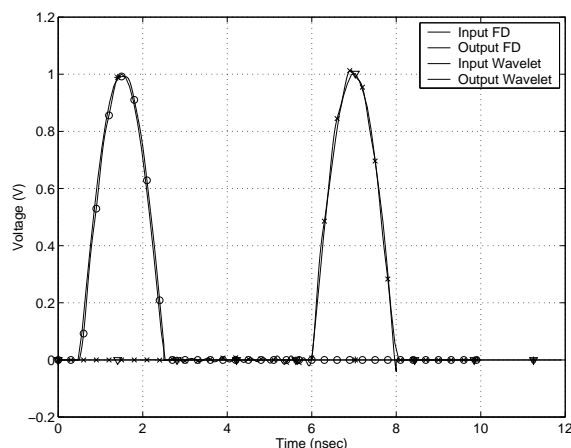


Figure 1: Input and output voltages of the lossless line

this case since an analytical solution is available, and the results have been compared given the same number

of samples in the frequency domain. In order to obtain results with the same accuracy a CPU time of one order of magnitude greater is necessary with a FD code. The main reason is that in order to obtain results with the same accuracy a greater number of spatial unknowns (around one order of magnitude) must be chosen. This fact shows the good interpolating properties of the wavelet basis.

## 4.2 Single conductor line

The nonuniform conductor line considered here is represented in figure 2 and it is characterized by the following parameters:

$$c(x) = \begin{cases} 1.621 & 0 \leq x \leq 1 \\ 2.413 - 0.792x & 1 \leq x \leq 2 \\ 0.829 & 2 \leq x \leq 3 \end{cases} \text{ pF/cm}$$

$$l(x) = \begin{cases} 2.09 & 0 \leq x \leq 1 \\ 0.545 + 2.763x - 1.838x^2 + 0.6168x^3 & 1 \leq x \leq 2 \\ 3.657 & 2 \leq x \leq 3 \end{cases} \text{ nH/cm}$$

$$r_{dc}(x) = \begin{cases} 4.0 & 0 \leq x \leq 1 \\ 2.4/(1 - 0.4x) & 1 \leq x \leq 2 \\ 12.0 & 2 \leq x \leq 3 \end{cases} \Omega/cm$$

$$g(x) = 0S/m$$

$$R_1 = R_2 = 10\Omega; \quad L = 3cm$$

The variation of  $r$  with the frequency is given by

$$r(x, \omega) = r_{dc}(x) + kr_{dc}(x)\sqrt{2j\omega} \quad (26)$$

where  $k = 0.417 \times 10^{-5}$

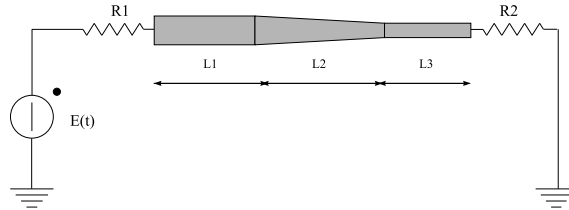


Figure 2: Single conductor nonuniform line

The input signal is an exponential function whose expression is  $E(t) = 1e^{-10t}$ .

Figures 3 show the input and output voltages of the line respectively with  $k = 0.417 \times 10^{-5}$  and  $k = 0$  (no frequency dependence). The results have been obtained with a number of wavelets equal to 256 and a CPU time of 12 minutes.

Comparing the two figures it can be noted the smoothing effect of the frequency dependence.

Figures 4 show the same results previously obtained but with a number of wavelet equal to 64 and a CPU time of 3 minutes. It can be noted that even with very few wavelet coefficients the results are clearly acceptable; furthermore the results remain stable as the number of wavelet coefficient increases. These are general trends observed in the considered tests.



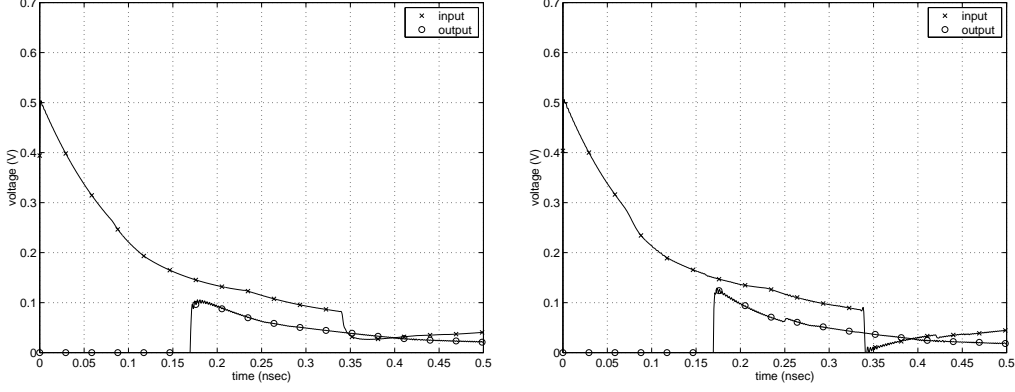


Figure 3: Input and output voltages with and without frequency dependence (n=256)

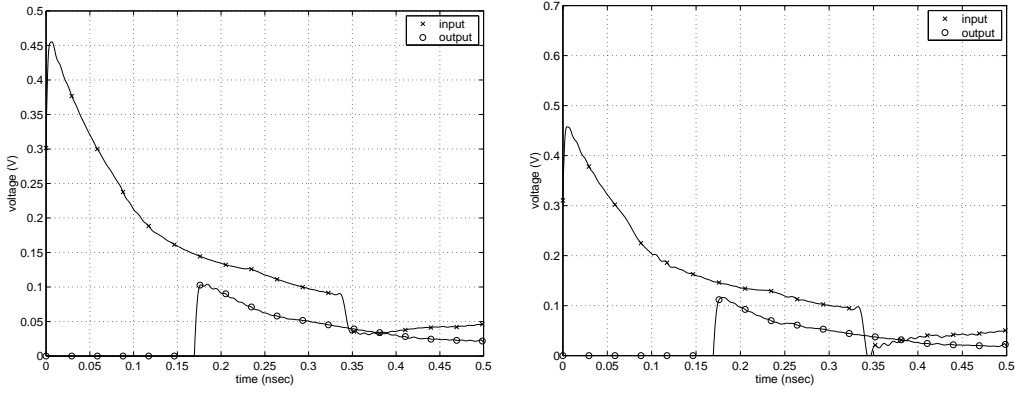


Figure 4: Input and output voltages with and without frequency dependence (n=64)

### 4.3 Multiconductor line

The behavior of a frequency dependent two conductor line has been investigated, both with a resistive load and a capacitive load.

#### 4.3.1 Resistive load

The nonuniform two conductor line considered here is represented in figure 5 and it is characterized by the following parameters:

$$c(x) = \begin{vmatrix} 122 & -50 \\ -50 & 122 \end{vmatrix} \left(1 + \frac{x}{L}\right)^{-2} pF/m$$

$$l(x) = \begin{vmatrix} 280 & 70 \\ 70 & 280 \end{vmatrix} \left(1 + \frac{x}{L}\right)^2 nH/m$$

$$g(x) = \begin{vmatrix} 2.3 & 0 \\ 0 & 2.3 \end{vmatrix} \left(1 + \frac{x}{L}\right)^{-2} \mu S/m$$

$$r_{dc}(x) = \begin{vmatrix} 0.2 & 0 \\ 0 & 0.2 \end{vmatrix} \left(1 + \frac{x}{L}\right)^2 \Omega/m$$

$$R_1 = R_2 = 10\Omega \quad R_3 = R_4 = 50\Omega$$

The line length is  $L = 3cm$  and the input signal is a half sine between time  $t = 0.2nsec$  and  $t = 0.4nsec$ . The variation of  $r$  with the frequency is given by:

$$r(x, f) = r_{dc}(x)(1 + k\sqrt{f}) \quad (27)$$

where  $k = 0.1$ .



Figure 5: Double conductor nonuniform line

Figures 6 show the input and output voltages at the ends of the line in case of frequency dependence:

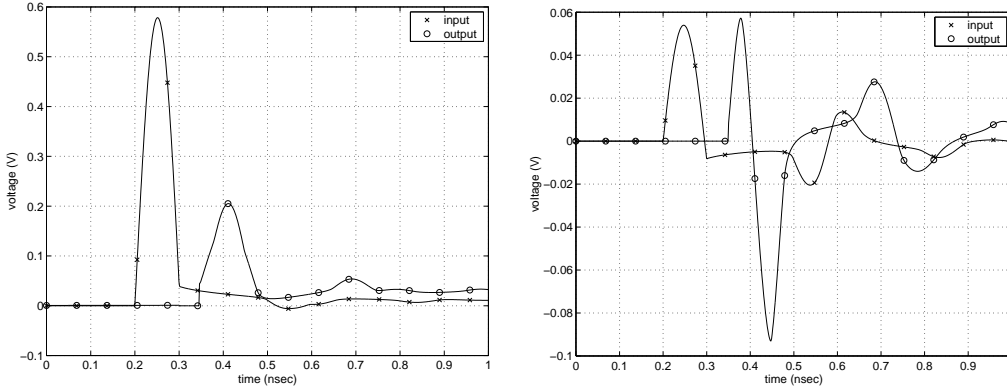


Figure 6: Input and output voltages of both conductor with frequency dependence

Figures 7 show the input and output voltages at the ends of the line in case of no frequency dependence:

In the two conductor line the results have been obtained with a number of wavelets equal to 128. The comparison between the figures shows again the smoothing effect of the frequency dependence.

#### 4.3.2 Capacitive load

The nonuniform two conductor line considered here is represented in figure 8 and the capacitive load (parallel between a resistor and a capacitor) is the representation of the nominal value of the input impedance of a CMOS inverter corresponding to  $1\mu m$  gate technology.

The line parameters are the same as before, with

$$R_4 = 1M\Omega, \quad C = 0.1pF$$

and the input and output voltages at both the conductors are investigated.

Figures 9 show the input and output voltages at the ends of the line in case of frequency dependence.

Figures 10 show the input and output voltages at the ends of the line in case of no frequency dependence:

The results show that the capacitive load enhances the signal transmission when the CMOS is energized, with respect to the results obtained in absence of capacitance. On the other hand the frequency dependence of the parameters has the same effect of reducing the amplitude of the transmitted signals.

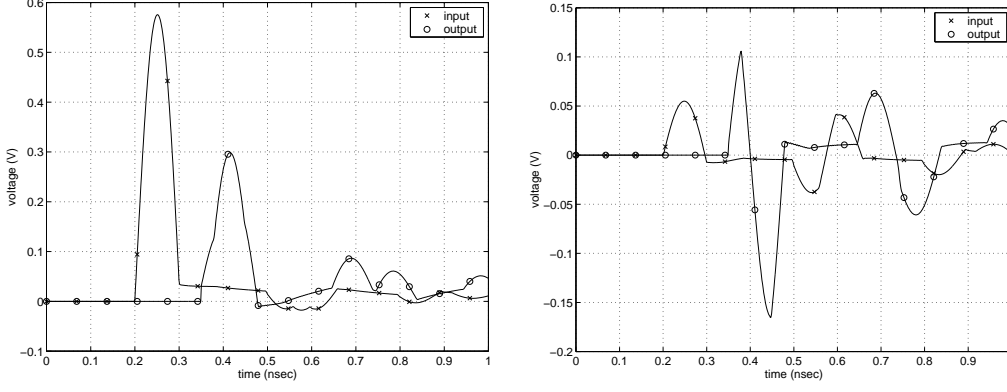


Figure 7: Input and output voltages of both conductors with no frequency dependence



Figure 8: Double conductor nonuniform line with capacitive load

Other tests have been performed on a uniform line having the same configuration of figure 8, characterized by the parameters:

$$c = \begin{vmatrix} 122 & -50 \\ -50 & 122 \end{vmatrix} pF/m \quad l = \begin{vmatrix} 280 & 70 \\ 70 & 280 \end{vmatrix} nH/m$$

$$g = \begin{vmatrix} 2.3 & 0 \\ 0 & 2.3 \end{vmatrix} \mu S/m \quad r_{dc} = \begin{vmatrix} 0.2 & 0 \\ 0 & 0.2 \end{vmatrix} \Omega/m$$

$$R_1 = R_2 = 10\Omega \quad R_3 = 50\Omega$$

$$R_4 = 1M\Omega, \quad C = 0.1pF$$

$$r(f) = r_{dc}(1 + k\sqrt{f}) \quad (28)$$

where  $k = 0.1$ . The line length is again  $L = 3cm$  and the input signal is the same as before.

Figures 11 show the input and output voltages at the ends of the line in case of frequency dependence:

Figures 12 show the input and output voltages at the ends of the line in case of no frequency dependence:

Comparing this last two figures (11 and 12) with (9 and 10) it can be seen that the effect of the frequency dependence is qualitatively the same one (signal smoothing and reduction) but it is more evident in a nonuniform line than in a uniform line. This trend is also shown in [6].

## 5 Conclusions

The method proposed here for the analysis of high speed interconnects with frequency dependent parameters is based on wavelet expansion in the space domain and FFT in the frequency domain. The tests performed on many cases have demonstrated that the method is efficient and reliable also with low memory and low CPU time requirements.

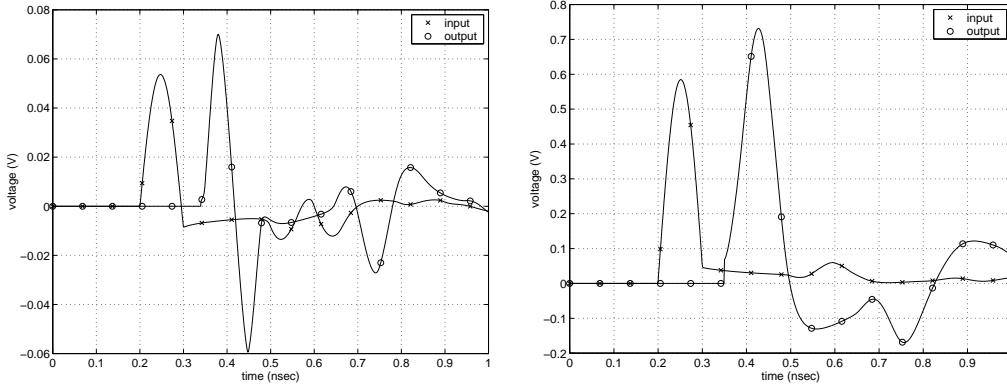


Figure 9: Input and output voltages of both conductors with frequency dependence

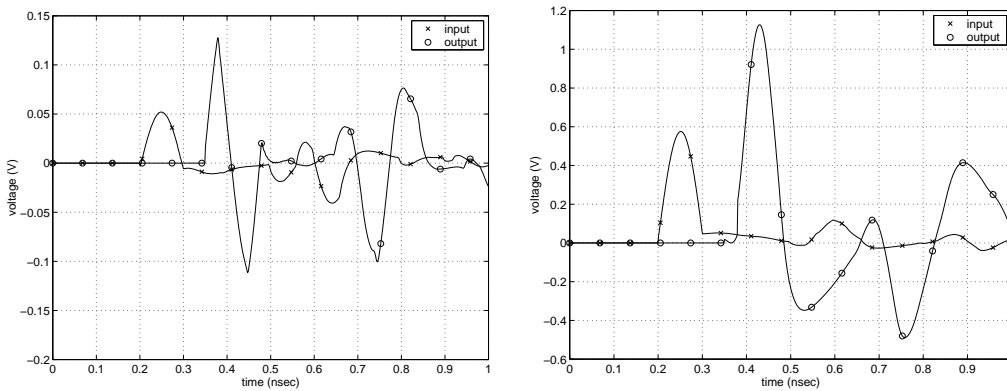


Figure 10: Input and output voltages of both conductors with no frequency dependence

## References

- [1] A. Djordjevic, T. Sarkar, "Analysis of time response of lossy multiconductor transmission line network" *IEEE Trans. MTT Vol 35, n. 10, Oct. 1987, pp 898-907.*
- [2] J. E. Shutt-Aine, "Transient analysis of nonuniform transmission lines" *IEEE Trans. CAS-1 Vol. 39 n. 5, May. 1992, pp 378-385.*
- [3] F. Y. Chang, "Transient simulation of nonuniform coupled lossy transmission lines characterized with frequency dependent parameters - part I: waveform relaxation analysis" *IEEE Trans. CAS-39, n. 8, August 1992, pp 585-603.*
- [4] E. C. Chang, S. M. Kang, "Computationally efficient simulation of a lossy transmission line with skin effect by using numerical inversion of laplace transform" *IEEE Trans. On CAS-1. Vol. 39, n. 11, Nov. 1992, pp 861-868.*
- [5] H. Heeb, A. E. Ruehli, "Three-dimensional interconnect analysis using partial element equivalent circuits" *IEEE Trans. On CAS-1. Vol. 39, n. 11, Nov. 1992, pp 974-982.*
- [6] V. K. Tripathi, N. Orhanovic, "Time - domain characterization and analysis of dispersive dissipative interconnects" *IEEE Trans. On CAS-1. Vol. 39, n. 11, Nov. 1992, pp 938-945.*
- [7] T. Dhaene, L. Martens, D. De Zutter, "Transient simulation of arbitrary nonuniform interconnection structures characterized by scattering parameters" *IEEE Trans. On CAS-1. Vol. 39, n. 11, Nov. 1992, pp 928-937.*

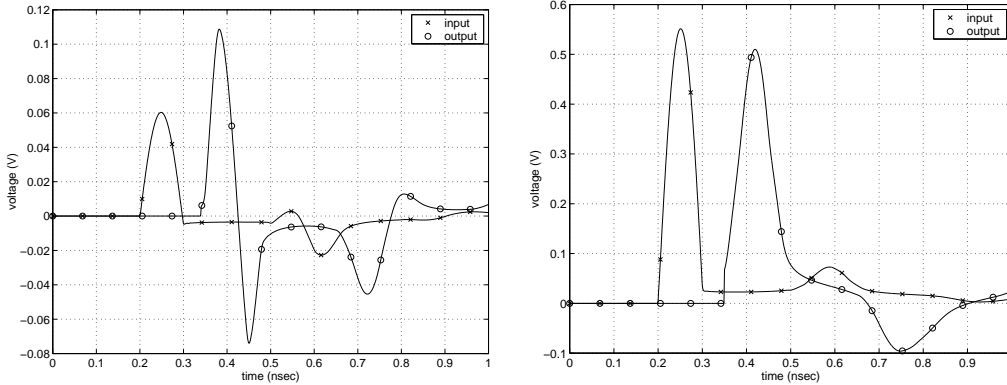


Figure 11: Input and output voltages of both conductors with frequency dependence

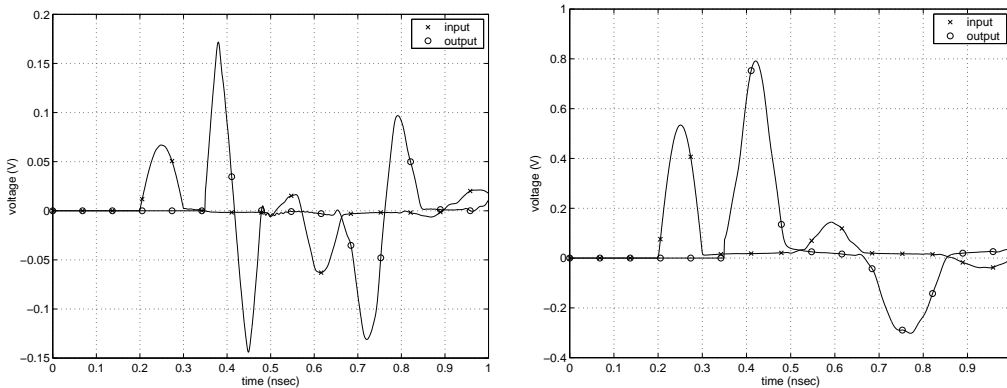


Figure 12: Input and output voltages of conductor 1 with no frequency dependence

- [8] F. Y. Chang, "Transient simulation of frequency - dependent nonuniform coupled lossy transmission lines" *IEEE Trans. On CPM Tech.- B. Vol. 17, n. 1, Feb. 1994, pp 3-14.*
- [9] L. Corti, G. Miano, L. Verolino "A new technique for simulating nonlinear loaded lossy lines" *IEEE Trans. MAG Vol. 32, n. 3, May 1996, pp 934-937.*
- [10] A. Orlandi, C. R. Paul, "FDTD analysis of lossy, multiconductor transmission lines terminated in arbitrary loads" *IEEE Trans. On EMC. Vol. 38, n. 3, Aug. 1996, pp 388-398.*
- [11] S. Grivet-Talocia, F. Canavero, "Wavelet-based adaptive solution for the nonuniform multiconductor transmission lines" *IEEE Microwave and Guided Wave Letters, vol.8, pp.287-289, August 1998.*
- [12] S. Barmada, M. Raugi, "Transient Numerical Solutions of nonuniform MTL equations with Nonlinear Loads by Wavelet Expansion in Time or Space Domain" " *IEEE Transactions on Circuits and Systems August 2000, Vol 47, n 8, pp-1178 - 1190*
- [13] S. Barmada, M. Raugi, "Space - time wavelet expansion iterative solution of nonuniform transmission lines with arbitrary loads" *International Journal of Numerical Modelling, Vol 28, n 3, 2001, pp 219-235*
- [14] C. K. Chui, "Wavelets: a tutorial in theory and applications" *New York, Academic Press, 1992.*
- [15] A.Cohen, I. Daubechies, B. Jawerth, P. Vial, "Multiresolution analysis wavelets and fast algorithms on the interval" *C. R. Acad. Sci. Paris ser. i Math. Vol 316, 1992, pp 417-421.*

- [16] T. K. Sarkar, C. Su, R. Adve, M. Salazar-Palma, L. Garcia-Castillo, R. R. Boix, "A tutorial on wavelets from an electrical engineering perspective, Part 1:Discrete Wavelet Techiques" *IEEE Antennas and Propagation Magazine*, Vol. 40, No 5, October 1998.
- [17] G. Beylkin "Wavelets and fast numerical algorithms" *Proc. of Symposia in Applied Math. Vol 47, 1993*
- [18] R. L. Wiginton, N. S. Nahman "Transient analysis of coaxial cables considering skin effect" *Proc IRE*, pp.166 - 174, Feb. 1957
- [19] N. S. Nahman, D. R. Holt "Transient analysis of coaxial cables using the skin effect approximation  $A + B\sqrt{s}$ " *IEEE Trans Circuit Theory*, vol CT - 19. pp. 443 -451, Sept. 1972

# Fast Multipole Formulation for PEEC Frequency Domain Modeling

Giulio Antonini

Dept. of Electrical Engineering,  
University of L'Aquila  
67040, Poggio di Roio, AQ, ITALY  
[antonini@ing.univaq.it](mailto:antonini@ing.univaq.it)

Keywords: Integral equations, Partial Element Equivalent Circuit Method, Fast Multipole Method.

## Abstract

This paper presents a tutorial and overview of the Fast Multipole Method (FMM) which is used to improve the performances of the Partial Element Equivalent Circuit (PEEC) technique in the frequency domain. Aim of the tutorial is to introduce the reader with the basic theory of the Fast Multipole Method. Step-by-step implementations of FMM are detailed providing useful guidelines for the potential user. The FMM is used in the PEEC framework showing how to compute PEEC parameters in a more efficient way without compromising the accuracy. Several examples are presented in which FMM has proven to be useful. A comprehensive list of references is also provided to allow the interested readers to go deeper inside FMM.

## 1 Introduction

Realistic Electromagnetic Compatibility (EMC) and Electrical Interconnect and Package (EIP) problems require flexible computational tools which can provide meaningful solutions for many different problems such as lightning, high frequency on-chip interconnects and Printed Circuit Board (PCB) modeling. Over the last few years the continuous increase of speed of digital electronic chips and increased frequencies of RF circuits has made their electromagnetic modeling an extremely challenging task. Clock rates of several hundred megahertz and signal rise/fall times of less than 100 ps cause the spectra of waveforms to extend up to 10 GHz. At these frequencies inductive and capacitive coupling between different conductors is no longer negligible and an accurate electromagnetic modeling is required to provide good simulations. In order to incorporate all the effects suitable models are required. On the other hand the intrinsic three-dimensional (3-D) nature of realistic problems limits the use of Transverse Electromagnetic waves (TEM) or quasi-TEM mode lumped circuit models. Among all the numerical methods of particular interest to high frequency high-speed mixed-signal circuit electrical analysis is the Partial-Element Equivalent Circuit (PEEC) method [1-3]. The PEEC formulation results in a circuit model which includes all the retardation effects. Moreover it is compatible with a non-linear circuit simulation framework like SPICE. These two features make the PEEC method especially tailored for studying mixed electromagnetic-circuit problems such as high-

speed electrical interconnect and package as well as for other EMC problems, such as power/ground-plane EMI de-coupling [4] and PCBs analysis.

This paper deals with the incorporation of the Fast Multipole Method (FMM) into the PEEC method in the frequency domain. In the last decade FMM has been widely used in conjunction with the Method of Moments (MoM) in the frequency domain for the analysis of scattering problems of electrically large objects [5,6]. More recently the FMM time domain counterpart has been developed by Michielsen's group [7-9] and adopted to study scattering from closed surfaces [10] and to analyze EMC/EMI problems [11]. As FMM is specially suitable for efficient computation of the dense matrix-vector product as those arising from integral methods it can be successfully used to enhance also the PEEC method. In particular in this tutorial paper FMM-based expressions of mutual partial inductances and potential coefficients are presented and it is shown how the proposed approach can speed-up their evaluation. As a consequence the matrix-vector products arising from the Modified Nodal Analysis (MNA) [12] are computed more efficiently.

The paper is organized as follows: Section 2 is devoted to a short overview of the PEEC method, then FMM theory is described in Section 3. The evaluation of PEEC parameters, partial inductances and potential coefficients, by using the FMM method is presented in Section 4; the FMM-based matrix-vector product scheme is assessed in Section 5; Section 6 describes several numerical results. Conclusions are summarized in Section 7.

## 2 PEEC theory

In the following it is assumed that the space is filled with an uniform dielectric although PEEC models have been developed also for finite dielectrics [3]. PEEC method is derived from the following equation to be enforced in the conductors and dielectrics

$$\hat{n} \times \left( -\vec{\mathbf{E}}_0(\vec{\mathbf{r}}, \omega) + \frac{\vec{\mathbf{J}}(\vec{\mathbf{r}}, \omega)}{\sigma} + j\omega\vec{\mathbf{A}}(\vec{\mathbf{r}}, \omega) + \nabla\Phi(\vec{\mathbf{r}}, \omega) \right) = 0 \quad (1)$$

where  $\vec{\mathbf{E}}_0$  denotes the external electric field,  $\vec{\mathbf{J}}$  is the current density in the conductor,  $\vec{\mathbf{A}}$  and  $\Phi$  are the magnetic vector and electric scalar potentials respectively. The magnetic vector potential  $\vec{\mathbf{A}}$  and the electric scalar potential  $\Phi$  at any point  $\vec{\mathbf{r}} = (\mathbf{x}, \mathbf{y}, \mathbf{z})$  are given by

$$\vec{\mathbf{A}}(\vec{\mathbf{r}}, \omega) = \frac{\mu}{4\pi} \int_{V'} G(\vec{\mathbf{r}}, \vec{\mathbf{r}}') \vec{\mathbf{J}}(\vec{\mathbf{r}}', \omega) dV' \quad \Phi(\vec{\mathbf{r}}, \omega) = \frac{1}{4\pi\epsilon} \int_{S'} G(\vec{\mathbf{r}}, \vec{\mathbf{r}}') \rho(\vec{\mathbf{r}}', \omega) dS' \quad (2)$$

where  $\rho$  the surface charge density and  $G$  the Green's function for an homogeneous medium

$$G(\vec{\mathbf{r}}, \vec{\mathbf{r}}') = \frac{e^{jk|\vec{\mathbf{r}}-\vec{\mathbf{r}}'|}}{|\vec{\mathbf{r}}-\vec{\mathbf{r}}'|} \quad (3)$$

Substituting the vector and scalar potentials into (1) yields the following integral equation



$$\hat{n} \times \left( -\vec{\mathbf{E}}_0(\vec{\mathbf{r}}, \omega) + \frac{\vec{\mathbf{J}}(\vec{\mathbf{r}}, \omega)}{\sigma} + j\omega\mu \int_V G(\vec{\mathbf{r}}, \vec{\mathbf{r}}') \vec{\mathbf{J}}(\vec{\mathbf{r}}', \omega) dV' + \frac{\nabla}{\epsilon} \int_{S'} G(\vec{\mathbf{r}}, \vec{\mathbf{r}}') \rho(\vec{\mathbf{r}}', \omega) dS' \right) = 0 \quad (4)$$

In order to solve integral equation (4) current and charge densities are discretized into volume and surface cells respectively. Applying Galerkin method allows obtaining PEEC models with conventional circuit elements. Ohmic losses are taken into account by longitudinal resistances, the magnetic field coupling is represented by means of partial inductances and the last term in equation (4) corresponds to the voltage drop expressed in terms of potential coefficients. Enforcing Kirchhoff's current law (KCL) to each node and Kirchhoff's voltage law (KVL) to each loop of the equivalent circuit leads to the standard MNA formulation [12].

$$\begin{bmatrix} -A & -R - j\omega L_p \\ j\omega P^{-1} + Y_{lumped} & -A^T \end{bmatrix} \begin{bmatrix} V \\ I_L \end{bmatrix} = \begin{bmatrix} V_s \\ I_s \end{bmatrix} \quad (5)$$

where  $A$  is the connectivity matrix,  $P$  is the potential coefficients matrix taking into account the electric field coupling,  $L_p$  is the partial inductances matrix which reproduces the magnetic field coupling,  $Y_{lumped}$  represents the admittance matrix of lumped elements,  $V_s$  and  $I_s$  are lumped voltage and current sources respectively,  $V$  and  $I_L$  are potentials to infinity and longitudinal currents. If charges  $Q$  are assumed as unknowns instead of potentials to infinity  $V$  the following alternative formulation is easily found

$$\begin{bmatrix} -AP & -R - j\omega L_p \\ j\omega \mathbf{\Pi} + Y_{lumped} P & -A^T \end{bmatrix} \begin{bmatrix} Q \\ I_L \end{bmatrix} = \begin{bmatrix} V_s \\ I_s \end{bmatrix} \quad (6)$$

The discretization of integral equation (4) thus gives rise to dense operator matrix. The solution of matrix equation (6) by iterative methods involves many matrix-vector products. This fact can make the solution extremely slow to be obtained when a large number of unknowns is considered and, hence, adopting a technique which enables to significantly accelerate the matrix fill-in process and the computation of matrix-vector products is highly desirable.

### 3 The Fast Multipole Method

The Fast Multipole Method was introduced by Rokhlin for acoustic wave scattering in two dimensions [13], Lu and Chew [5] applied the FMM method in electromagnetics to compute the scattered field of two-dimensional dielectric coated conducting cylinders and Coifman, Rokhlin and Wandzura [14] extended it to the three-dimensional wave equation. In 1995 Song and Chew [6] introduced a multilevel-FMM based algorithm. More recently Michielssen, Ergin and Shanker proposed its direct time-domain counterpart known as Plane-Wave Time Domain algorithm (PWTD) [7-11]. FMM has been mainly applied to scattering problems that are usually solved writing the corresponding integral equation assuming the induced current distribution as unknown. The Method of Moments (MoM) is used to convert the integral equation to a matrix equation. Scattering computation from large objects is a hard task because of the huge number of unknowns. Solving the matrix equation by means of LU decomposition requires  $O(N^3)$  operations. In this case iterative solvers such as the Conjugate Gradient

(CG) allow reducing computational complexity to  $O(N^2)$  operations per iteration, since the most costly step is the matrix vector multiplication which becomes the bottleneck. FMM has been found to be effective in speeding-up this process. In the present paper FMM is used to accelerate the computation of PEEC parameters, namely partial inductances  $L_p$  and potential coefficients  $P$  and, as a consequence, the matrix-vector products which involve these matrices such as  $L_p I_L$  and  $PQ$  in Equation (6) can be performed in a more efficient way.

The evaluation of these matrix-vector products allows obtaining the effect at each location of basis functions of currents  $I_L$  or charges  $Q$  due to all the currents  $I_L$  or charges  $Q$  themselves. A matrix-vector product involving a dense matrix and a dense vector requires  $N^2$  operations, as illustrated in Fig. 1.

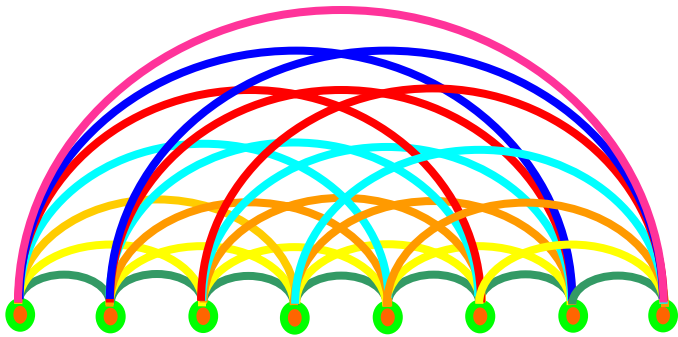


**Fig. 1** - One level interaction: all sources “talk” directly to each other. The number of links is proportional to  $N^2$  where  $N$  is the number of sources.

Every source communicates with each other source directly. If the sources are grouped together into  $G$  groups, the number of the interactions can be significantly reduced. Fig. 2 shows the resulting two-level structure of the interaction among the sources. This type of approach is based on certain decomposition of the kernel of the original integral problem. The decomposition reduces the connections among basis functions belonging to different groups and this is the reason of the speed-up that the FMM techniques provide in computing matrix-vector products.

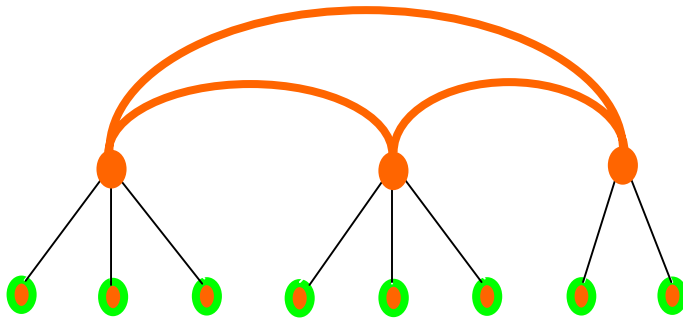


**Fig. 2** - Two level interaction: sources “talk” indirectly to each other. The number of links is proportional to  $G^2$  where  $G$  is the number of groups of sources.

The Fast Multipole Method (FMM) is based on two elementary identities which can be found in many texts and handbooks on mathematical methods such as [15] and [16]. Let's consider a target

(observation ) point  $\vec{\mathbf{r}}_m$  and a source point  $\vec{\mathbf{r}}_n$ . The first expansion represents the Green's function by using the Gegenbauer's addition theorem:

$$\frac{e^{jk_0|\vec{\mathbf{r}}_m-\vec{\mathbf{r}}_n|}}{|\vec{\mathbf{r}}_m-\vec{\mathbf{r}}_n|} = \frac{e^{jk_0|\vec{\mathbf{R}}+\vec{\mathbf{d}}|}}{|\vec{\mathbf{R}}+\vec{\mathbf{d}}|} = j k_0 \sum_{l=0}^{\infty} (-1)^l (2l+1) j_l(k_0 d) h_l^{(1)}(k_0 R) P_l(\hat{\mathbf{d}} \cdot \hat{\mathbf{R}}), \quad R > d \quad (7)$$

where  $j_l$  is a spherical Bessel function of the first kind,  $h_l^{(1)}$  is a spherical Hankel function of the first kind and  $P_l$  is a Legendre polynomial and  $R > d$ . The second expansion allows to expand the product  $j_l(k_0 d) P_l(\hat{\mathbf{d}} \cdot \hat{\mathbf{R}})$  in propagating plane waves as follows:

$$j_l(k_0 d) P_l(\hat{\mathbf{d}} \cdot \hat{\mathbf{R}}) = \frac{1}{4\pi j^l} \int_{S^2} e^{j\vec{\mathbf{k}}_0 \cdot \vec{\mathbf{d}}} P_l(\hat{\mathbf{k}}_0 \cdot \hat{\mathbf{R}}) d^2 \hat{\mathbf{k}}_0 \quad (8)$$

where  $\vec{\mathbf{k}}_0 = k_0 \hat{\mathbf{k}}_0$  and the notation  $\int_{S^2} \cdot d^2 \hat{\mathbf{k}}_0$  stands for integration over the unit sphere:

$$\int_{S^2} \cdot d^2 \hat{\mathbf{k}}_0 = \int_0^{2\pi} \int_0^\pi \sin \theta d\theta d\phi \quad \text{and} \quad \hat{\mathbf{k}}_0 = \sin \theta \cos \phi \hat{x} + \sin \theta \sin \phi \hat{y} + \cos \theta \hat{z} \quad (9)$$

Combining Equations (7) and (8) we obtain:

$$\frac{e^{jk_0|\vec{\mathbf{r}}_m-\vec{\mathbf{r}}_n|}}{|\vec{\mathbf{r}}_m-\vec{\mathbf{r}}_n|} = \frac{j k_0}{4\pi} \int_{S^2} e^{j\vec{\mathbf{k}}_0 \cdot \vec{\mathbf{d}}} \left[ \sum_{l=0}^{\infty} j^l (2l+1) h_l^{(1)}(k_0 R) P_l(\hat{\mathbf{k}}_0 \cdot \hat{\mathbf{R}}) \right] d^2 \hat{\mathbf{k}}_0 \quad R > d \quad (10)$$

In accordance with the FMM the  $N$  unknowns of the problem (currents or charges), introduced for the discretization of equation (4) are subdivided into  $G$  groups, with each group assigned  $M=N/G$  unknowns. Let's assume that the target (observation ) point  $\vec{\mathbf{r}}_m$  belongs to a group with a center  $\vec{\mathbf{r}}_a$  and the source point  $\vec{\mathbf{r}}_n$  belongs to a group with center  $\vec{\mathbf{r}}_b$ . Thus we may write

$$\vec{\mathbf{r}}_m - \vec{\mathbf{r}}_n = \vec{\mathbf{R}} + \vec{\mathbf{d}} = (\vec{\mathbf{r}}_m - \vec{\mathbf{r}}_a) + (\vec{\mathbf{r}}_a - \vec{\mathbf{r}}_b) + (\vec{\mathbf{r}}_b - \vec{\mathbf{r}}_n) = \vec{\mathbf{r}}_{ma} + \vec{\mathbf{r}}_{ab} - \vec{\mathbf{r}}_{nb} \quad (11)$$

where  $\vec{\mathbf{r}}_a - \vec{\mathbf{r}}_b \equiv \vec{\mathbf{r}}_{ab} = \vec{\mathbf{R}}$  and  $(\vec{\mathbf{r}}_m - \vec{\mathbf{r}}_a) - (\vec{\mathbf{r}}_n - \vec{\mathbf{r}}_b) = \vec{\mathbf{r}}_{ma} - \vec{\mathbf{r}}_{nb} \equiv \vec{\mathbf{d}}$ . The approximation of the Green's function (3) is established from an elementwise approximation. To obtain an elementwise expansion we use the source center  $\vec{\mathbf{r}}_b$  and the target center  $\vec{\mathbf{r}}_a$  as the reference points and expand the Green's function about  $\vec{\mathbf{r}}_a - \vec{\mathbf{r}}_b$ , see Fig. 3.

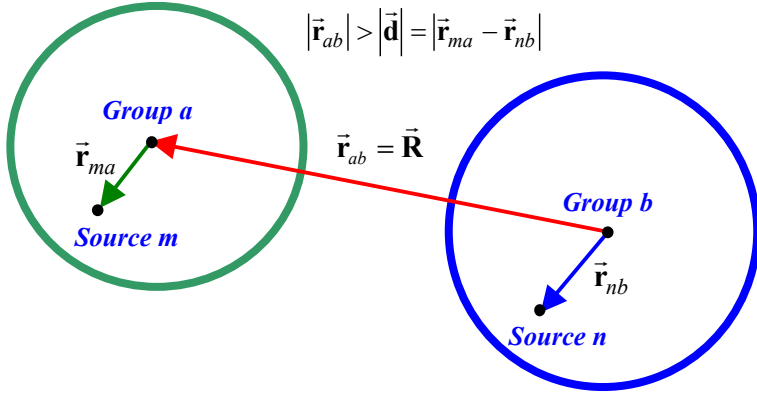


**Fig. 3** – Expansion about  $\vec{r}_a - \vec{r}_b$  and separation of  $\vec{r}_{ma}$  and  $\vec{r}_{nb}$ .

Truncating the infinite sum in (7) by retaining only  $L+1$  terms leads to the following approximation of the scalar Green's function

$$\begin{aligned} \frac{e^{jk_0|\vec{r}_m - \vec{r}_n|}}{|\vec{r}_m - \vec{r}_n|} &\cong \frac{jk_0}{4\pi} \int_{k_0} e^{j\vec{k}_0 \cdot (\vec{r}_{ma} - \vec{r}_{nb})} \left[ \sum_{l=0}^L j^l (2l+1) h_l^{(1)}(k_0 R) P_l(\hat{\mathbf{k}}_0 \cdot \hat{\mathbf{R}}) \right] d^2 \hat{\mathbf{k}}_0 \\ &= \frac{jk_0}{4\pi} \int_{S^2} e^{j\vec{k}_0 \cdot (\vec{r}_{ma} - \vec{r}_{nb})} \alpha_{ab}^L(\hat{\mathbf{R}} \cdot \hat{\mathbf{k}}_0) d^2 \hat{\mathbf{k}}_0 \end{aligned} \quad (12)$$

where

$$\alpha_{ab}^L(\hat{\mathbf{R}} \cdot \hat{\mathbf{k}}_0) = \sum_{l=0}^L j^l (2l+1) h_l^{(1)}(k_0 R) P_l(\hat{\mathbf{k}}_0 \cdot \hat{\mathbf{R}}), \quad a, b=1, \dots, G \quad (13)$$

The number of the  $L+1$  terms to be retained depends on the desired accuracy. The integration in Equation (12) is done numerically. There several possibilities for the choice of sample points on the unit sphere  $S^2$ . The most straightforward is the uniform distribution of points:

$$\phi_i = \frac{2\pi}{I} i \quad \theta_j = \frac{\pi}{J} j \quad (14)$$

being  $I$  and  $J$  the number of sampling points of  $\phi \in [0 - 2\pi]$  and  $\theta \in [0 - \pi]$ .

This choice has the clear advantage of being simple but doesn't allow a very accurate integration of spherical harmonics. It requires twice more points than the Gauss-Legendre points. The optimal choice of sample points are uniform points for  $\phi$  and Gauss-Legendre points for  $\theta$ . With this choice of points it is possible to integrate exactly all the spherical harmonics of order  $L$  using  $L+1$  points in the  $\theta$  direction and  $2L+2$  points in the  $\phi$  direction.

The function  $\alpha_{ab}^L(\hat{\mathbf{R}} \cdot \hat{\mathbf{k}}_0)$  is defined for each different groups pair and it depends on the unit vector  $\hat{\mathbf{k}}_0$ . Fig. 4 shows the behavior of function  $\alpha_{ab}^L(\hat{\mathbf{R}} \cdot \hat{\mathbf{k}}_0)$  for  $L=14$ ,  $k_0 R=30$  and different values of the angle between  $\hat{\mathbf{R}}$  and  $\hat{\mathbf{k}}_0$ , being  $\cos\theta = \hat{\mathbf{R}} \cdot \hat{\mathbf{k}}_0$ .

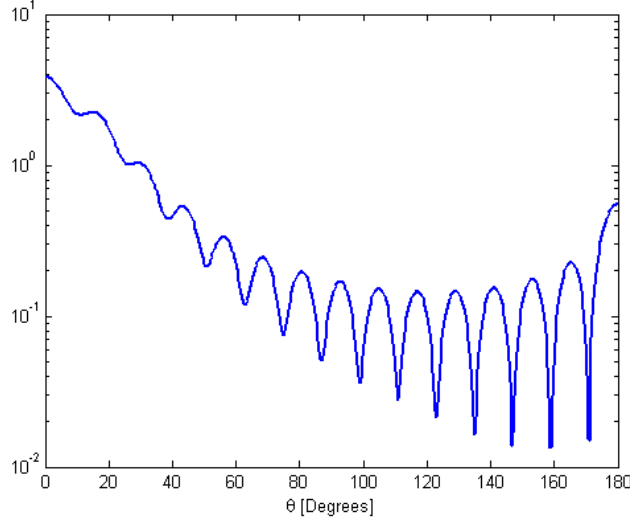


**Fig. 4** – Amplitude of  $\alpha_{ab}^L(\hat{\mathbf{R}} \cdot \hat{\mathbf{k}}_0)$  in Equation (13) as function of  $\theta$  for  $L=14$  and  $k_0 R=30$  where  $\cos\theta = \hat{\mathbf{R}} \cdot \hat{\mathbf{k}}_0$ .

#### 4 PEEC parameters computation

The above outlined approach to represent the Green's function can be used to obtain approximated coefficients describing the electromagnetic coupling. According to the PEEC method the magnetic and electric field couplings are described by partial inductances  $L_p$  and potential coefficients  $P$  matrices which must be evaluated to fill in the MNA matrix (5) or (6). FMM allows representing these matrices separating the contribution due to basis functions (currents and charges) belonging to groups satisfying the condition  $R > d$  (non-near neighbors) from that of groups which don't accomplish it (near neighbors). Furthermore the first contribution is factorized in such a way to de-couple the sources. If  $A$  is the generic matrix describing the coupling, by using the FMM expansion it can be expressed as

$$A = A^{near} + A^{far} \quad (15)$$

and  $A^{far}$  matrix entries can be factored as  $A_{mn}^{far} = \bar{V}_{ma}^t \tilde{\alpha}_{ab} \bar{V}_{nb}$ , where indexes  $a$  and  $b$  refer to groups to which sources  $m$  and  $n$  belong. A plane-wave basis has proven to diagonalize the matrix  $\tilde{\alpha}_{ab}$ . This result was originally achieved by Rokhlin [13]. As a consequence of that the non-near neighbors contribution is factorized into a product of a vector, a diagonal matrix and a vector. It is worth to note that vectors  $\bar{V}_{ma}^t$  and  $\bar{V}_{nb}$  can be re-used in computing all the interactions involving sources  $m$  and  $n$  respectively and need to be computed just once at the beginning. Furthermore it is also possible to pre-compute the function  $\tilde{\alpha}_{ab}$ , as it will be clarified in the following Sections.

## 4.1 Partial inductances computation

The standard expression for volume mutual partial inductances between two different inductive cells  $m$  and  $n$  is given by

$$L_{p,mn} = \frac{\mu \cos \theta_{mn}}{4\pi S_m S_n} \int_{V_m} \int_{V_n} G(\vec{\mathbf{r}}_m, \vec{\mathbf{r}}_n) dV_m dV_n \quad (16)$$

where  $\cos \theta_{mn}$  takes into account the direction of current basis functions  $m$  and  $n$ .

Let's assume that inductive cells  $m$  and  $n$  belong to groups  $a$  and  $b$  which satisfy the condition  $R > d$  required by the spectral representation (10) to be valid. Under this hypothesis, taking into account the approximated form of the free space Green's function  $G(\vec{\mathbf{r}}_m, \vec{\mathbf{r}}_n)$  given by Equation (12) we can rewrite the partial inductance  $L_{p,mn}$  as:

$$L_{p,mn} = \frac{jk_0 \mu \cos \theta_{mn}}{(4\pi)^2 S_m S_n} \int_{k_0} \left[ \int_{V_m} e^{j\vec{k}_0 \cdot \vec{\mathbf{r}}_{ma}} dV_m \right] \alpha_{ab}^L(\hat{\mathbf{r}}_{ab} \cdot \hat{\mathbf{k}}_0) \left[ \int_{V_n} e^{-j\vec{k}_0 \cdot \vec{\mathbf{r}}_{nb}} dV_n \right] d^2 \hat{\mathbf{k}}_0 \quad (17)$$

This expression can be rewritten in a more compact form in terms of volume field and source functions  $F_m^v(\hat{\mathbf{k}}_0)$  and  $S_n^v(\hat{\mathbf{k}}_0)$  respectively which are scalar functions of  $\hat{\mathbf{k}}_0$  defined for every cells pair  $m$  and  $n$ .

$$F_m^v(\hat{\mathbf{k}}_0) = \int_{V_m} e^{j\vec{k}_0 \cdot \vec{\mathbf{r}}_{ma}} dV_m, \quad m = 1, \dots, N \quad (18a)$$

$$S_n^v(\hat{\mathbf{k}}_0) = \int_{V_n} e^{-j\vec{k}_0 \cdot \vec{\mathbf{r}}_{nb}} dV_n = F_m^{v*}(\hat{\mathbf{k}}_0) \quad n = 1, \dots, N \quad (18b)$$

where  $\vec{\mathbf{r}}_{ma}$  and  $\vec{\mathbf{r}}_{nb}$  are the relative vectors of cells  $m$  and  $n$  with respect to the centers of groups  $a$  and  $b$  to which they belong. Substituting Equations (18a,b) into Equation (17) yields

$$\begin{aligned} L_{p,mn} &= \frac{jk_0 \mu \cos \theta_{mn}}{(4\pi)^2 S_m S_n} \int_{k_0} F_m^v(\hat{\mathbf{k}}_0) \alpha_{ab}^L(\hat{\mathbf{r}}_{ab} \cdot \hat{\mathbf{k}}_0) S_n^v(\hat{\mathbf{k}}_0) d^2 \hat{\mathbf{k}}_0 \\ &= \frac{jk_0 \mu \cos \theta_{mn}}{(4\pi)^2 S_m S_n} \int_{k_0} F_m^v(\hat{\mathbf{k}}_0) \alpha_{ab}^L(\hat{\mathbf{r}}_{ab} \cdot \hat{\mathbf{k}}_0) F_m^{v*}(\hat{\mathbf{k}}_0) d^2 \hat{\mathbf{k}}_0 \end{aligned} \quad (19)$$

which represents the FMM approximation of the partial inductance  $L_{p,mn}$ .

## 4.2 Potential coefficients computation

Similarly the PEEC method models electric field coupling between conductive regions  $m$  and  $n$  by means of potential coefficient  $P_{mn}$  given by a double folded surface integral as

$$P_{mn} = \frac{1}{4\pi \varepsilon A_m A_n} \int_{A_m} \int_{A_n} G(\vec{\mathbf{r}}_m, \vec{\mathbf{r}}_n) dA_m dA_n \quad (20)$$

where  $A_m$  and  $A_n$  represent surface areas of patches  $m$  and  $n$ . Under the same hypothesis ensuring the validity of Gegenbauer's addition theorem, a multipole representation of potential coefficient  $P_{mn}$  can be obtained. Using the Green's function approximation given by Equation (12), truncating the infinite sum in (12) to the first  $L+1$  terms leads to the following form of potential coefficient  $P_{mn}$ :

$$P_{mn} = \frac{jk_0}{(4\pi)^2 \varepsilon A_m A_n} \int_{k_0} \left[ \int_{A_m} e^{j\hat{\mathbf{k}}_0 \cdot \vec{\mathbf{r}}_{ma}} dA_m \right] \alpha_{ab}^L(\hat{\mathbf{r}}_{ab} \cdot \hat{\mathbf{k}}_0) \left[ \int_{A_n} e^{-j\hat{\mathbf{k}}_0 \cdot \vec{\mathbf{r}}_{nb}} dA_n \right] d^2 \hat{\mathbf{k}}_0 \quad (21)$$

Two auxiliary functions can be defined as

$$F_m^S(\hat{\mathbf{k}}_0) = \int_{S_m} e^{j\hat{\mathbf{k}}_0 \cdot \vec{\mathbf{r}}_{ma}} dA_m, \quad m = 1, \dots, N \quad (22a)$$

$$S_n^S(\hat{\mathbf{k}}_0) = \int_{S_n} e^{-j\hat{\mathbf{k}}_0 \cdot \vec{\mathbf{r}}_{nb}} dA_n = F_n^{S*}(\hat{\mathbf{k}}_0) \quad n = 1, \dots, N \quad (22b)$$

Equation (21) can be rewritten in a more compact form as

$$\begin{aligned} P_{mn} &= \frac{jk_0}{(4\pi)^2 \varepsilon A_m A_n} \int_{k_0} F_m^S(\hat{\mathbf{k}}_0) \alpha_{ab}^L(\hat{\mathbf{r}}_{ab} \cdot \hat{\mathbf{k}}_0) S_n^S(\hat{\mathbf{k}}_0) d^2 \hat{\mathbf{k}}_0 = \\ &= \frac{jk_0}{(4\pi)^2 \varepsilon A_m A_n} \int_{k_0} F_m^S(\hat{\mathbf{k}}_0) \alpha_{ab}^L(\hat{\mathbf{r}}_{ab} \cdot \hat{\mathbf{k}}_0) F_n^{S*}(\hat{\mathbf{k}}_0) d^2 \hat{\mathbf{k}}_0 \end{aligned} \quad (23)$$

It is worth to remind that representations (19) and (23) are valid when the distance between the two groups  $\vec{\mathbf{R}} = \vec{\mathbf{r}}_{ab}$  is greater than the distance  $\vec{\mathbf{d}} = |\vec{\mathbf{r}}_{ma} - \vec{\mathbf{r}}_{nb}|$ . For the cells belonging to groups not satisfying that condition, matrix entries  $L_{mn}$  and  $P_{mn}$  must be evaluated by the rigorous formulas (16) and (20).

### 4.3 Elementwise expansion of FMM-PEEC parameters

The matrix interpretation of FMM-based computation of PEEC parameters can be found. The matrix interpretation of one-dimensional FMM of complexity  $O(n \log n)$  is well presented in [19]. A matrix version of FMM for the Laplace equation can be found in [20]. It is useful to give the same perspective also in the computation of PEEC parameters. The matrix version is more than a mere replacement for multiple summations and recursions by a clean matrix notation. The matrix viewpoint may help make the FMM more understandable to scientists and engineers who may want to use FMM for their computations.

The basic idea of the FMM is to establish a matrix factorization from an analytic elementwise expansion. This means that the FMM allows representing the Green's function in terms of matrix products.

Let us consider two basis functions whose centers  $\vec{r}_m$  and  $\vec{r}_n$  are well separated in the sense that conditions for applying the Gegenbauer's addition theorem are satisfied. As stated above the integration on the unit sphere is performed by using Gauss-Legendre integration with  $L+1$  points for the integral over  $\theta$  and uniform integration with  $2(L+1)$  points for the integral over  $\phi$ . Let us assume as auxiliary variable  $u = \cos\theta = \hat{\mathbf{k}}_0 \cdot \hat{\mathbf{R}} \in [-1, 1]$ , let  $w_u$  and  $w_\phi$  be the row vectors of the quadrature weights,  $\Delta u$  and  $\Delta\phi$  the angular step for the integration over  $u$  and  $\phi$  respectively. Furthermore, for a fixed order  $L$  of the multipole expansion, functions  $F_m^v(\hat{\mathbf{k}}_0)$ ,  $S_n^v(\hat{\mathbf{k}}_0)$ ,  $F_m^S(\hat{\mathbf{k}}_0)$  and  $S_n^S(\hat{\mathbf{k}}_0)$  can be regarded as matrices of order  $(L+1) \times (2L+2)$ . For a pair of inductive or capacitive cells  $m$  and  $n$  belonging to two well separated groups  $a$  and  $b$  function  $\alpha_{ab}^L$  is also represented by a matrix of order  $(L+1) \times (2L+2)$  when the vector  $\hat{\mathbf{k}}_0$  varies on the unit sphere. It is clearly seen that the computation of the mutual partial inductance  $L_{p,mn}$  and potential coefficient  $P_{mn}$  by FMM can be re-cast in a matrix form as

$$L_{p,mn} = \cos\theta_{mn} w_\phi \Delta\phi (F_m^v \square \alpha_{ab}^L \square S_n^v) w_u^T \Delta u \quad (24a)$$

$$P_{mn} = w_\phi \Delta\phi (F_m^S \square \alpha_{ab}^L \square S_n^S) w_u^T \Delta u \quad (24b)$$

where  $\square$  denotes the Hadamard (elementwise) product of two matrices.

## 5 Fast matrix-vector product

It is well known that solving matrix equations arising from integral methods such as PEEC becomes more and more time demanding with the increase of the number of unknowns. When the discretization of the integral equation results in a total number of unknowns larger than some thousands direct solvers are not useful and iterative methods must be used. Their computational cost is  $O(N^2)$ ,  $N$  being the matrix order and it is equal to the cost of a single full matrix-vector multiplication. Obviously it is important to speed-up this product as much as possible. In applying the MNA it is required calculating many matrix-vector products, involving the partial inductances  $L_p$  and potential coefficients  $P$  matrices. Evaluating a matrix-vector multiplication is equal to compute the effect at a given observation point  $\vec{r}$  due to all the sources, currents and charges. For a single observation point the contribution from neighbor groups is evaluated by using the exact formula given by (16) and (20). The contribution from far groups is calculated using the FMM-based formulas (19) and (23). The two terms are finally added to obtain the total effect. In the following we will refer to the matrix-vector product  $j\omega L_p I_L$  but the same considerations can be done for the  $PQ$  product.

The idea is to divide the current sources into  $G$  groups. Each of them contains approximately  $N/G$  cells. Let us denote  $G_a$  the set of cells which belong to group  $a$ . For each group of cells the near and far field region are found. Let  $N_a$  the set of groups which are near neighbors to group  $a$ .

$$N_a = \{b : |\vec{r}_a - \vec{r}_b| \leq R\} \quad a = 1, \dots, G \quad (25)$$



where  $R$  is the distance beyond which two groups are considered far neighbors.

In order to better explain how the method works let us consider the relation giving the magnetic vector potential at location  $\vec{r}_m$  belonging to group  $G_a$  generated by the current flowing in the cell  $n$  belonging to group  $G_b$ .

$$\vec{\mathbf{A}}(\vec{r}_m, \vec{r}_n) = \frac{\mu}{4\pi} \int_{V_n} G(\vec{r}_m, \vec{r}_n) \vec{\mathbf{J}}(\vec{r}_n) dV_n \quad (26)$$

The total magnetic vector potential due to all the current sources can be calculated considering separately the contributions from the near neighbors groups and that from far groups. This can be done mathematically as

$$\begin{aligned} \vec{\mathbf{A}}(\vec{r}_m) = & \sum_{b \in N_a} \sum_{n \in G_b} \frac{\mu}{4\pi S_n} \int_{V_n} G(\vec{r}_m, \vec{r}_n) i_n \hat{\mathbf{u}}_n dV_n + \\ & + \frac{\mu}{4\pi} \int_{k_0} e^{j\vec{k}_0 \cdot \vec{r}_{ma}} \sum_{b \notin N_a} \alpha_{ab}^L(\hat{\mathbf{r}}_{ab} \cdot \hat{\mathbf{k}}_0) \left[ \sum_{n \in G_b} \left( \frac{1}{S_n} \int_{V_n} e^{-j\vec{k}_0 \cdot \vec{r}_{nb}} dV_n \right) i_n \hat{\mathbf{u}}_n \right] \quad \text{for } m = 1, \dots, N \end{aligned} \quad (27)$$

where it has been assumed  $\vec{\mathbf{J}}(\vec{r}_n) \cong \frac{i_n}{S_n} \hat{\mathbf{u}}_n$ . It can be easily seen that the evaluation of the contribution of the far groups to the magnetic vector potential at point  $\vec{r}_m$  is carried out in three steps. In the first one it is calculated the field at each group center due to the sources of the group.

$$\vec{\mathbf{A}}_1(\vec{r}_b, k_0) = \left[ \sum_{n \in G_b} \left( \frac{1}{S_n} \int_{V_n} e^{-j\vec{k}_0 \cdot \vec{r}_{nb}} dV_n \right) i_n \hat{\mathbf{u}}_n \right] \quad \text{for } b = 1, \dots, G \quad (28)$$

In the second stage the field is translated from one group's center to another one. This is represented by the calculation of

$$\vec{\mathbf{A}}_2(\vec{r}_a, k_0) = \sum_{b \notin N_a} \alpha_{ab}^L(\hat{\mathbf{r}}_{ab} \cdot \hat{\mathbf{k}}_0) \vec{\mathbf{A}}_1(\vec{r}_b, k_0) \quad \text{for } a = 1, \dots, G \quad (29)$$

In the last step the field at each group center is scattered to each cell inside the group as follows:

$$\vec{\mathbf{A}}_3(\vec{r}_m) = \frac{\mu}{4\pi} \int_{k_0} e^{j\vec{k}_0 \cdot \vec{r}_{ma}} \vec{\mathbf{A}}_2(\vec{r}_a, k_0) d^2\hat{\mathbf{k}}_0 \quad \text{for } m = 1, \dots, N \quad (30)$$

The total magnetic vector potential at point  $\vec{r}_m$  can be finally obtained as

$$\vec{\mathbf{A}}(\vec{r}_m) = \sum_{b \in N_a} \sum_{n \in G_b} \frac{\mu}{4\pi S_n} \int_{V_n} G(\vec{r}_m, \vec{r}_n) i_n \hat{\mathbf{u}}_n dV_n + \vec{\mathbf{A}}_3(\vec{r}_m) \quad \text{for } m = 1, \dots, N \quad (31)$$

In accordance to the standard PEEC method the inner product of a vector function  $\vec{f}$  with the unit vector  $\hat{\mathbf{u}}_m$  is defined as

$$\langle \vec{f} | \hat{\mathbf{u}}_m \rangle = \frac{1}{S_m} \int_{V_m} \vec{f}(\vec{r}_m) \cdot \hat{\mathbf{u}}_m dV_m \quad (32)$$

The inner product of  $\vec{\mathbf{A}}(\vec{r}_m)$  with  $\hat{\mathbf{u}}_m$  yields

$$\begin{aligned} \langle \vec{\mathbf{A}}(\vec{r}_m) | \hat{\mathbf{u}}_m \rangle &= \sum_{b \in N_a} \sum_{n \in G_b} \frac{\mu}{4\pi S_m S_n} \int_{V_m} \int_{V_n} G(\vec{r}_m, \vec{r}_n) i_n \hat{\mathbf{u}}_m \cdot \hat{\mathbf{u}}_n dV_m dV_n + \\ &+ \frac{1}{S_m} \int_{V_m} \hat{\mathbf{u}}_m \cdot \vec{\mathbf{A}}_3(\vec{r}_m) dV_m \quad \text{for } m \in G_a, n \in G_b \end{aligned} \quad (33)$$

The induced voltage on the inductive cell  $m$  due to all the current basis functions is obtained as

$$\begin{aligned} \sum_n j\omega L_{p,mn} I_{L,n} &= j\omega \sum_n \langle \vec{\mathbf{A}}(\vec{r}_m) | \hat{\mathbf{u}}_m \rangle = j\omega \sum_{b \in N_a} \sum_{n \in G_b} \frac{\mu}{S_m S_n} \int_{V_m} \int_{V_n} G(\vec{r}_m, \vec{r}_n) i_n \hat{\mathbf{u}}_m \cdot \hat{\mathbf{u}}_n dV_m dV_n + \\ &+ \frac{j\omega}{S_m} \int_{V_m} \hat{\mathbf{u}}_m \cdot \vec{\mathbf{A}}_3(\vec{r}_m) dV_m \quad \text{for } m = 1, \dots, N \end{aligned} \quad (34)$$

where  $\hat{\mathbf{u}}_m \cdot \hat{\mathbf{u}}_n = \cos\theta_{mn}$  takes into account the angle between the direction of the current basis functions  $m$  and  $n$ . Equation (34) provides a multipole representation of the magnetic field coupling between currents. The first term in equation (34) represents the contribution from the near neighbors groups, including the self group and the self cell. The second term in equation (34) takes into account the contribution from non-near neighbors groups. The same procedure can be applied to compute the potentials to infinity induced by charges, expressed by the matrix vector product  $PQ$ .

## 6 Numerical results

The accuracy of the computation of magnetic and electric field coupling in the PEEC method depends on the precision achieved in approximating the scalar Green's function by using Equation (12). In [17] it is shown that, if the number of digits of accuracy in the truncated Green's function is  $d_0$ , the order of expansion is given by  $L = k_0 d + 1.8d_0^{2/3} (k_0 d)^{1/3}$ .

As a first test the scalar Green's function has been computed using an expansion order  $L=7$ ,  $\vec{r}_{ab} = \vec{\mathbf{R}} = R \hat{\mathbf{z}}$ ,  $\vec{\mathbf{d}} = 0.4\lambda \hat{\mathbf{z}}$ . Fig. 4 shows magnitude (4a) and phase (4b) of the Green's function

evaluated by the exact formula (3) and that by means of (12) as function of the electrical distance between groups  $R/\lambda$ . Fig. 5 shows the relative error for various numbers of  $L$ .

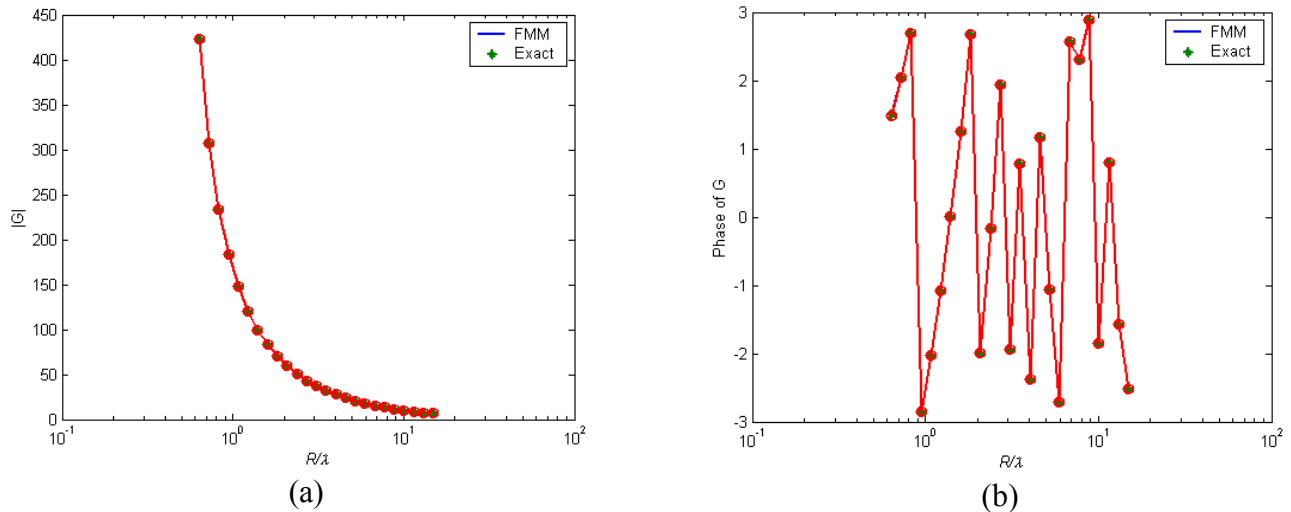


**Fig. 4** – Green’s function FMM approximation: (a) magnitude, (b) phase.

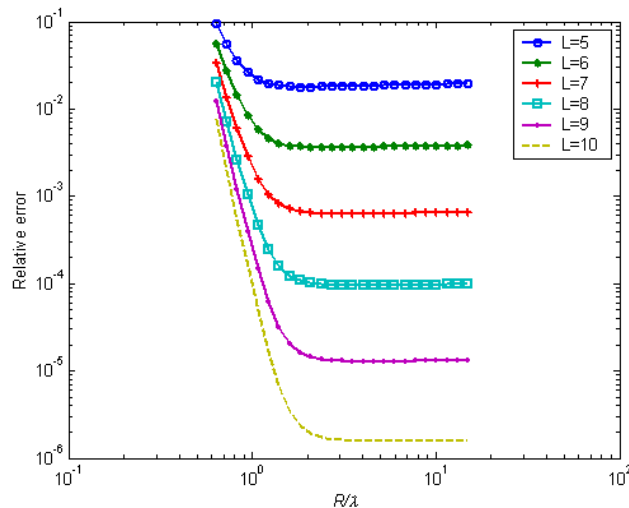


**Fig. 5** – Relative error in the Addition Theorem for different number of terms.

As clearly seen the scalar Green’s function is approximated accurately also for small electrical distances between groups ( $R \approx \lambda$ ).

The second test has been done comparing partial inductances computed by means of Equation (16) and the FMM-based one (19) for various electrical distances between the corresponding groups. Two inductive cells  $m$  and  $n$ , of length  $\lambda/10$  and cross section  $\lambda/10 \times \lambda/100$  have been considered. By using the same notation as before, referring to the center of the basis functions domain,  $\vec{r}_m - \vec{r}_n = \vec{R} + \vec{d}$  is assumed such that  $d$  is small enough to make  $R$  be close at  $|\vec{r}_m - \vec{r}_n|$ . Group center locations have been chosen such that  $d=0.4\lambda$ . Expansion order  $L=7$  has been adopted. Fig. 6 shows

magnitude (6a) and phase (6b) of the mutual partial inductance  $L_{p,mn}$  as function of the electrical distance between the groups.

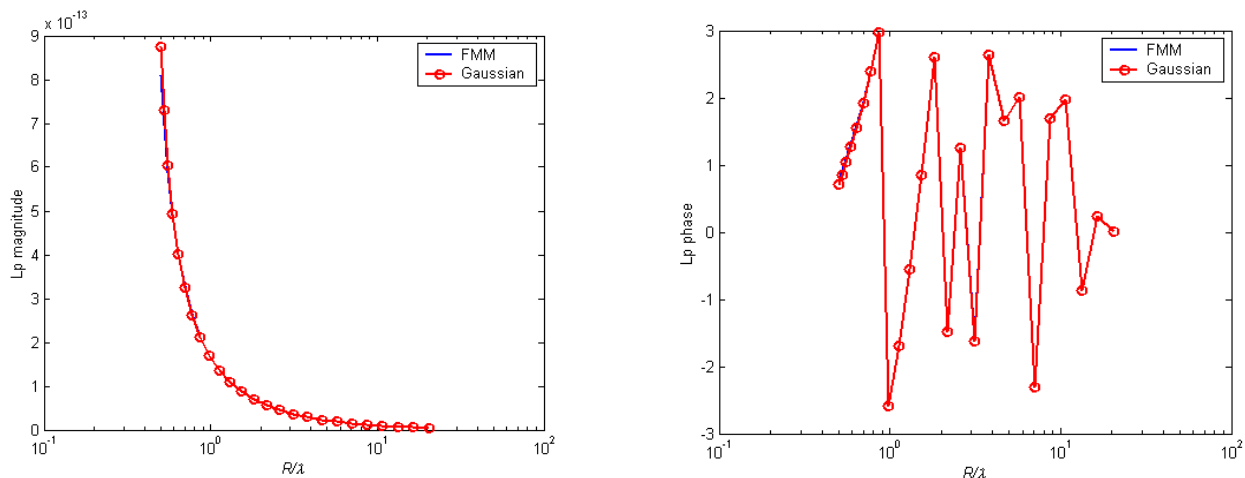


**Fig. 6** – Partial inductances computation ( $L=7$ ).

Further the relative error in the evaluation of  $L_{p,mn}$  for different number of terms in the truncated series is shown in Fig. 7.

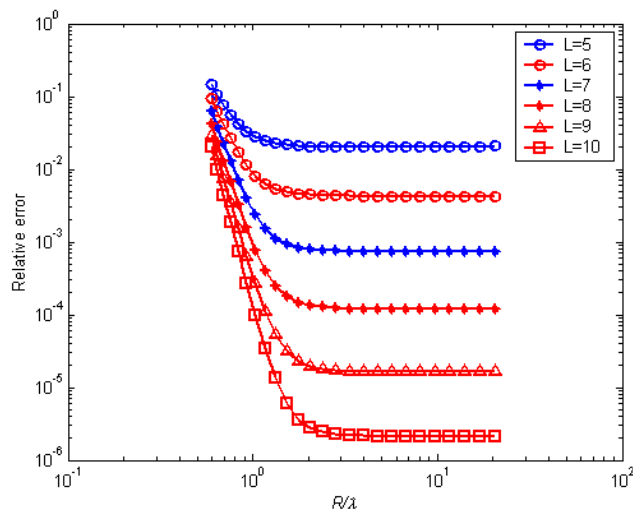


**Fig. 7** – Relative error in the computation of partial inductances.

Even in this case a very good accuracy can be obtained also for electrically close groups. Further examples and tests cases can be found in [18].

As final test partial inductances have been computed for different angular positions as shown in Fig. 8. Cells are  $\lambda/10$  long and are characterized by a  $\lambda/10 \times \lambda/100$  cross-section. Basis function have been chosen such that  $|\vec{r}_m - \vec{r}_n| = 2\lambda$  and  $d=0.4\lambda$  for all the different locations. Group centers are indicated by stars.

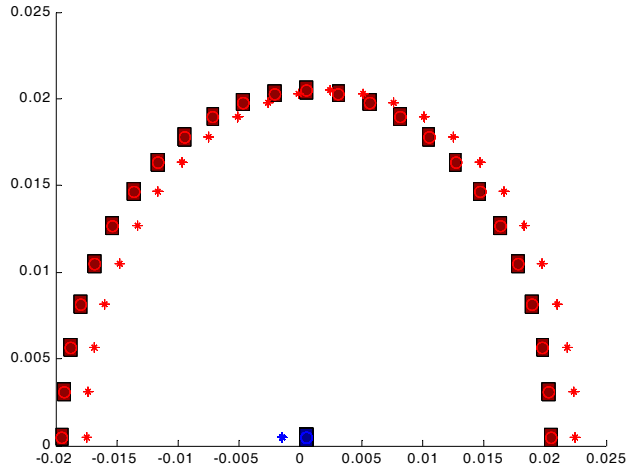


**Fig. 8** – Basis function and group centers locations.

The corresponding values of magnitude and phase of partial inductances obtained by means of Gauss-Legendre integration and FMM are sketched in Fig. 9. The numerical integral (17) has been performed using an eight order Gauss-Legendre integration, FMM has been applied with  $L=10$ . As seen the accuracy is good for both magnitude and phase of  $L_{p,mn}$ .

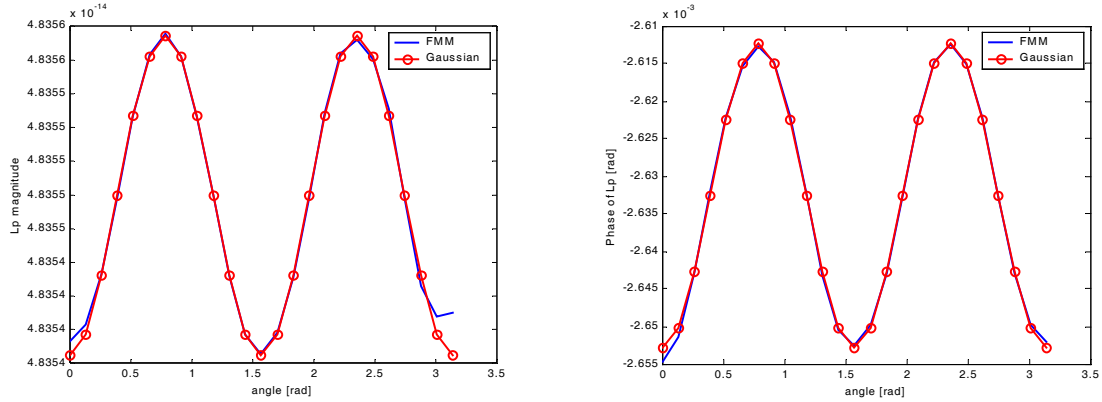


**Fig. 9** – Partial inductance computation ( $L=10$ ).

Finally the relative order in the computation of partial inductances  $L_{p,mn}$  has been evaluated for different numbers of terms  $L$  in the range [5-10]. Two cell dimensions have been considered,  $\lambda/4 \times \lambda/4$  and  $\lambda/10 \times \lambda/10$  respectively, in order to investigate the impact of the cell dimension on the accuracy. The thickness is  $0.01\lambda$ . The results are plotted in Fig. 10 confirming that acceptable  $10^{-3}$  accuracy is obtained for orders  $L$  larger than 7 for both the dimensions.

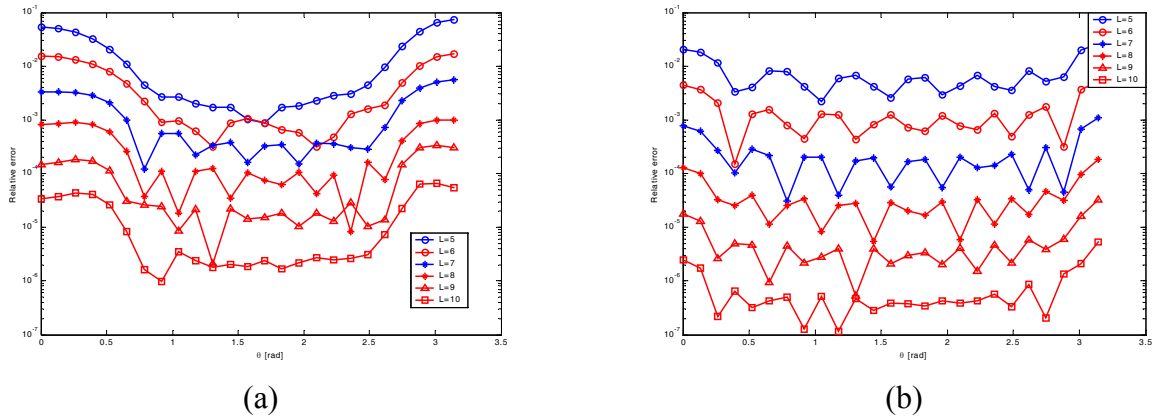


**Fig. 10** – Relative error for different expansion orders and cell dimension:  
(a)  $\lambda/4$ , (b)  $\lambda/10$  .

## 7 Conclusions

The paper has presented the application of the Fast Multipole Method to the Partial Element Equivalent Circuit Method. The use of the Addition Theorem allows to approximate the scalar Green's function in an accurate way introducing a de-coupling between non-near neighbor basis functions. A step-by-step implementation of coupling coefficients computation and matrix-vector product was then presented leading to multipole expressions for partial inductances and potential coefficients and a fast scheme to perform matrix-vector products as those arising from the MNA formulation. Several test have confirmed that good accuracy are achieved with relatively small orders of expansion.

## References

- [1] A.E. Ruehli, "Equivalent circuit models for three-dimensional multiconductor systems" *IEEE Trans. Microwave Theory Tech.*, vol. 22, n. 3, March 1974, pp 216-221.
- [2] H.Heeb, A.E. Ruehli, "Three-Dimensional Interconnect Analysis Using Partial Element Equivalent Circuit" *IEEE Trans. on Circuits and Systems-1: Fundamental Theory and Applications*, vol.39, no. 11, November 1992, pp.974-981.
- [3] A.E. Ruehli and H. Heeb, "Circuit Models for Three-Dimensional Geometries Including Dielectrics" *IEEE Trans. Microwave Theory Tech.*, vol. 40, n. 3, July 1992, pp. 1507-1516.
- [4] Archambeault B., A. E. Ruehli, "Analysis of power/ground-plane EMI decoupling performance using the partial-element equivalent circuit technique", *IEEE Transactions on Electromagnetic Compatibility*, vol. 43, no.4, November 2001.
- [5] C.C. Lu and W.C. Chew, "Fast algorithm for solving hybrid integral equations", *IEE Proceedings-H*, vol. 140, no. 6, pp.455-460, Dec. 1993.
- [6] J.M. Song and W.C. Chew, "Multilevel fast-multipole algorithm for solving combined field integral equations of electromagnetic scattering", *Microwave Opt. Technol. Lett.*, vol.10, no.1, pp. 14-19, Sept. 1995.
- [7] A.A. Ergin, B. Shanker, E. Michielssen, "The Plane-Wave Time-Domain Algorithm for the Fast Analysis of Transient Wave Phenomena", *IEEE Antennas Propagation Magazine*, vol. 41, no. 4, August 1999.

- [8] B. Shanker, A.A. Ergin, E. Michielssen, "A Multilevel Plane Wave Time Domain Algorithm for the Fast Analysis of Transient Scattering Phenomena", in *Proceedings of IEEE Antennas Propagat. Soc. Int. Symp.*, vol. 2, pp.1342-1345, Orlando, FL, July 11-16,1999.
- [9] B. Shanker, A.A. Ergin, K. Aygün, E. Michielssen, "Analysis of Transient Electromagnetic Scattering Phenomena Using a Two-Level Plane Wave Time Domain Algorithm", *IEEE Transactions on Antennas and Propagation*, vol. 48, no. 4, April 2000, pp. 510 – 523.
- [10] B. Shanker, A.A. Ergin, K. Aygün, E. Michielssen, "Analysis of Transient Electromagnetic Scattering from Closed Surfaces using a Combined Field Integral Equation", *IEEE Transactions on Antennas and Propagation*, vol. 48, no. 7, July 2000.
- [11] K. Aygun, B. Shanker, A.A. Ergin, E. Michielssen, "A Two Level Plane Wave Time Domain Algorithm for Fast Analysis of EMC/EMI Problems" *IEEE Transactions on Electromagnetic Compatibility*, vol. 44, no.1, February 2002.
- [12] C. Ho, A. Ruehli, P. Brennan, "The Modified Nodal Approach to Network Analysis", *IEEE Transactions on Circuits and Systems*, vol. CAS-22, pp. 504-509, June 1975.
- [13] V. Rokhlin, "Rapid solution of integral equations of scattering theory in two dimensions", *J. Comput. Phys.*, vol. 86, no.2, pp. 414-439, Feb. 1990.
- [14] R. Coifman, V. Rokhlin, S. Wandzura, "The Fast Multipole Method for the Wave Equation: a Pedestrian Description", *IEEE Trans. Antennas Propagat.*, vol. 35, no. 3, pp.7-12, June 1993.
- [15] M. Abramowitz and I.A. Stegun, *Handbook of Mathematical Functions*, New York: Dover Publications, 1972.
- [16] G. Arfken, *Mathematical Methods for Physicists*, New York, NY, Academic Press, second edition, 1970.
- [17] W.C. Chew, J.-M. Jin, E. Michielssen, J. Song, *Fast and Efficient Algorithms in Computational Electromagnetic*, Artech House, 2001.
- [18] G. Antonini, "The Fast Multipole Method for PEEC Circuits Analysis" in *Proc. of 2002 IEEE International Symposium on EMC*, Minneapolis, USA, August 2002.
- [19] L. Greengard, V. Rokhlin, "A Fast Algorithm for Particle Simulations", *Journal of Computational Physics*, (135):pp. 280-292, 1997.
- [20] X. Sun, N. P. Pitsianis, "A Matrix Version of the Fast Multipole Method", *SIAM Review*, 43(2):pp. 289-299, September 2001.

## Application of Some Common Numerical Methods to Simple Radiation and Scattering Problems

David C. Jenn  
jenn@nps.navy.mil

Yeo Chee Beng  
ycheeben@starnet.gov.sg

Sample calculations using three commonly used numerical methods are presented for some simple radiation and scattering problems. The three methods are: the method of moments (MM), the finite element method (FEM) and the finite integration technique (FIT). For the most part, standard software packages are used in the comparison:

*PATCH* – a Sandia Labs code based on the Rao, Wilton, Glisson triangular subdomains

*HFSS* – High Frequency Structures Simulator by Ansoft Corporation

*Microwave Studio* – by Computer Simulation Technology (CST)

The problems examined are:

1. The radiation from and impedance of an isolated dipole in free space,
2. An array of three dipoles over a finite perfect electric conductor (PEC) ground plane, and
3. The bistatic radar cross section (RCS) of a PEC plate.

For convenience all dimensions throughout are in meters and a frequency of 300 MHz is used so that 1 m corresponds to 1 wavelength.

Among the issues discussed are methods of exciting the structures, how to compute impedance, and the convergence of the solutions. This is not meant to be a rating of the software packages. Clearly each one has advantages and disadvantages in specific cases, and the engineer must determine the most efficient solution method for the particular problem at hand. A survey of the numerical methods such as this one can serve as a good introductory tutorial of computational electromagnetics (CEM) techniques in a university EM course.

### A. Method of Moments

The method of moments is in widespread use in various forms. As applied in most cases, the method of moments is used to convert the E-field integral equation (EFIE) into a set of simultaneous linear equations that can be solved by standard matrix techniques. The subdomains typically used for three-dimensional conducting structures are the triangular surface patches introduced by Rao, Wilton and Glisson [1]. Previous to that, wire approximations were common, such as those employed in the Numerical Electromagnetics Code (*NEC*).

The code *PATCH*, which originates from Sandia Labs, is one of many that use the triangular subdomains [2]. *PATCH* has a limited geometry builder that creates simple objects and combines them to form more complicated bodies. The facet models used here were generated in the computer aided design software *ACADS*. A translator program is then used to convert the *ACADS* “.facet” format into a format accepted by *PATCH*.



An efficient way of modeling a thin wire with circular cross section is to use a flat strip with an equivalent width determined by the wire diameter. A rule of thumb is that the equivalent circular radius is approximately 0.225 of the width,  $a_e \approx 0.225w$  [3]. *PATCH* has the ability to essentially break the surface at an edge (even if it is not a physical edge) and apply a voltage source or lumped load across the gap. If a 1 volt source is applied across edge number  $n$ , then the surface current crossing the edge  $J_n$  (A/m) can be determined from the MM expansion coefficients. Subsequently the current is computed from  $I_n = J_n \ell_n$  (A) where  $\ell_n$  is the length of the edge  $n$ . The ratio of voltage to current gives the impedance across the edge. Figure 1 shows the thin strip model. The voltage is applied to the center edge.

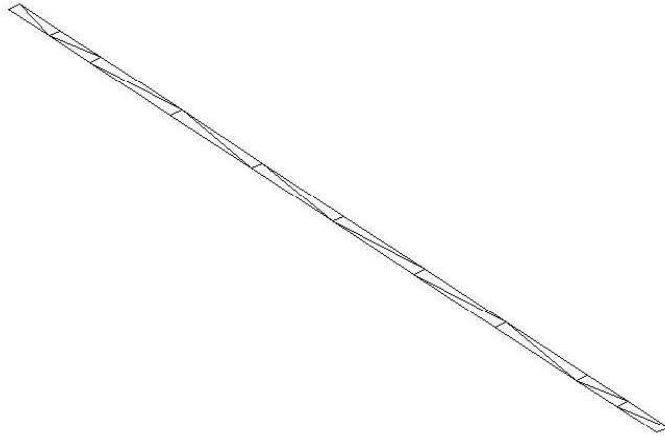


Figure 1: Example of a strip dipole meshed for the method of moments solution.

Extensive comparisons between the strip model and the *NEC* wire have been made [4]. The impedance and radiation patterns have been found to be essentially identical. For example, for a dipole of length 0.45 m and 0.00125 m in diameter, the impedance computed by *PATCH* is  $58.3-j55.9$  versus  $61.8-j43.4$  ohms by *NEC*. By slightly reducing the length of the *NEC* wire to 0.44m the agreement is within a couple of tenths of an ohm.

A three element array of dipoles over a finite ground plane is shown in Figure 2. The dipoles are aligned with the  $z$  axis and spaced 0.4 m. The height of the dipoles above the ground plane is 0.25 m and the ground plane has dimensions 1.5 m in  $x$  and 1 m in  $z$ . The dipoles are excited with equal voltages and the H-plane pattern ( $\theta = 90^\circ$ ) is shown in Figure 3 for terminal loads of  $R_L = 0, 50, \text{ and } 100000$  ohms. The latter case approximates an open circuit condition. There are approximately 3500 edges in the model, with the maximum edge length of 0.063 m, which is less than the 0.1 wavelength rule of thumb for convergence at the  $-30$  dB level.

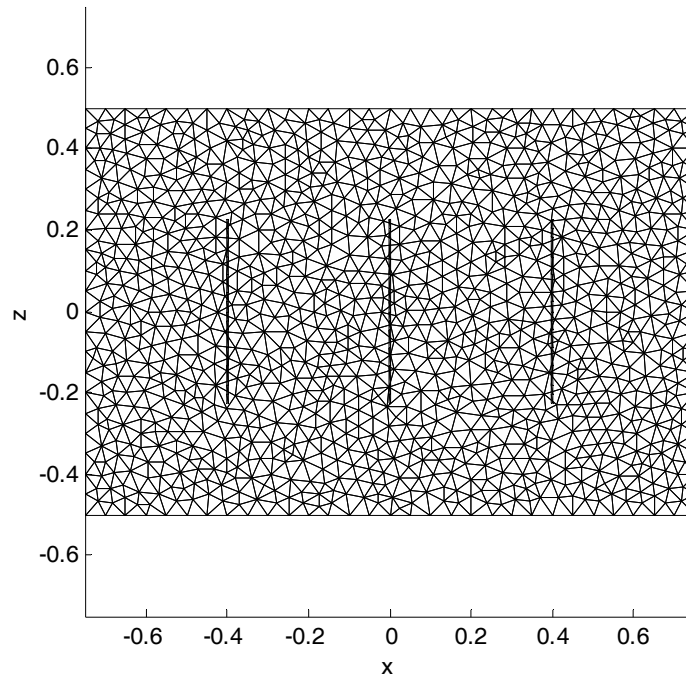


Figure 2: Array of dipoles over a finite ground plane showing triangular subdomains.

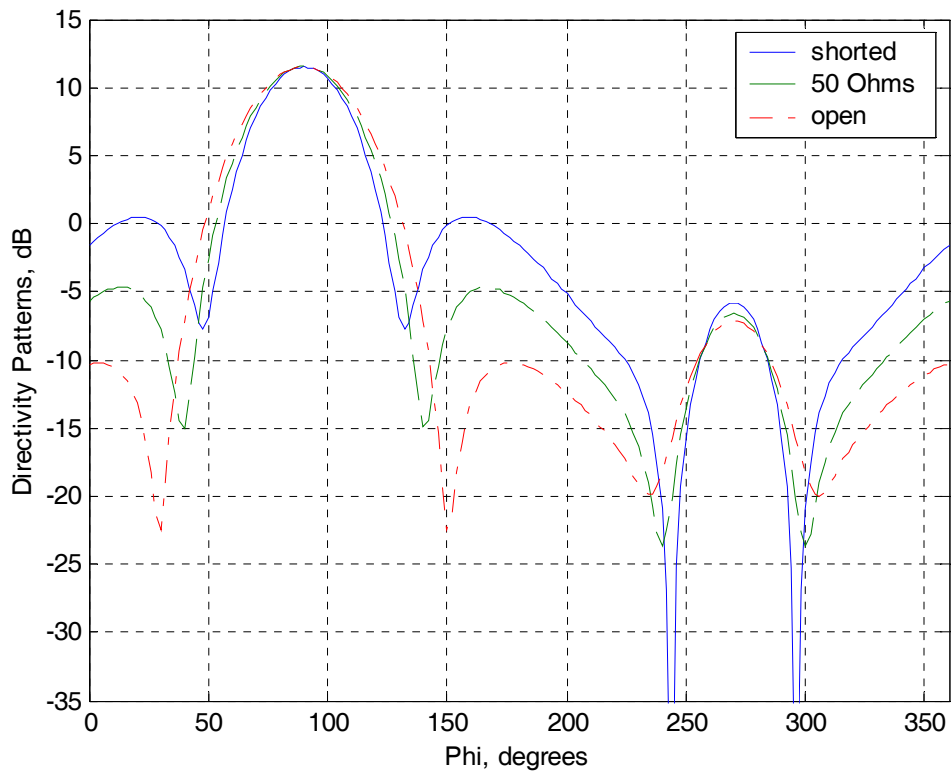


Figure 3: Method of moments patterns for three load conditions.

## B. Finite Element Method

The finite element method (FEM) is perhaps the oldest numerical technique used in engineering applications. FEM has been used more extensively for EM problems in recent years due to the development of vector basis functions and effective methods of treating the computational boundaries [5]. The boundary conditions are necessary when applying the FEM to radiation and scattering problems.

Ansoft's High Frequency Structures Simulator (*HFSS*) was used for FEM calculations [6]. *HFSS* has a geometry builder, adaptive meshing, and a powerful post processor. The FEM model of the dipole is shown in Figure 4. The computational "air box" is slightly greater than 0.25 m on all sides (0.25 wavelength is the general rule of thumb for placement of the radiation boundaries from the structures).

Although *HFSS* is capable of modeling the details of the feed, such as the coaxial feed line and balun, the simplest feed arrangement possible was considered for this study. This would be desirable, for example, when an array is being integrated into a platform and the platform effects on the array pattern are of interest. A simple feed model would require less computer memory than a detailed one, thereby freeing up computational resources for more detail in the platform and antenna structure models.

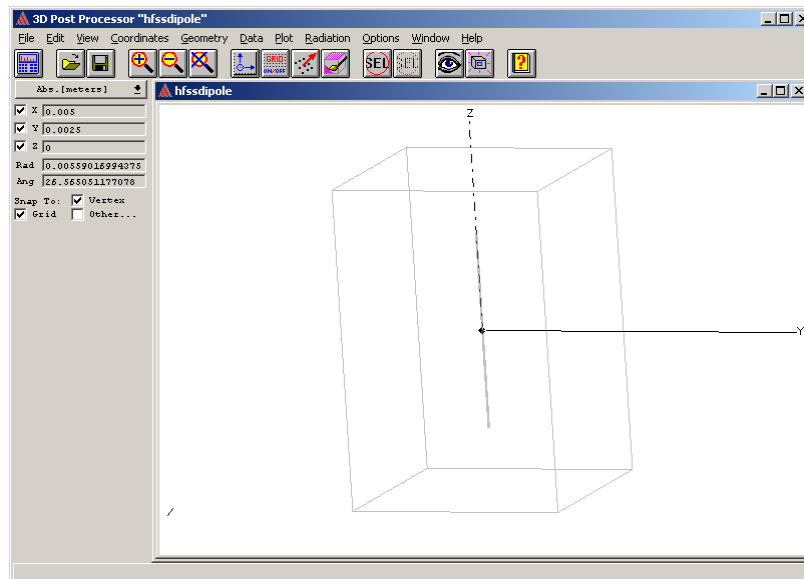


Figure 4: *HFSS* model of the dipole and radiation box.

*HFSS* has current and voltage gap sources that can be used to excite the dipoles. Lumped *RLC* elements can be applied as boundaries. The *HFSS* dipole model is a circular cylinder of diameter 0.00125 m and a total length of 0.45 m. A gap of 0.01 m is cut at the center and a rectangle spans the gap as shown in Figure 5. A 1 A current source is applied on the rectangle and electric field in the gap computed. To obtain the impedance, the "calculator" functions are used to integrate the field in the gap between the dipole arms. The resulting voltage divided by the current source gives the impedance. Using this technique an impedance of  $55.6-j32$  was

obtained for the isolated dipole. (A more direct approach would be to use a lumped gap source type of port, which does not require using the calculator to integrate the field in the gap.)

For the array calculation a 1.5 m by 1 m ground plane was added 0.25 m from the dipoles as shown in Figure 6. The ground plane has a finite thickness of 0.01 m. The lumped  $RLC$  boundary is applied to a second rectangle in the gap that is perpendicular to the first rectangle on which the current source was applied (see Figure 7). The H-plane pattern is shown in Figure 8 for several mesh densities, and in Figure 9 for load conditions of  $R_L = 0.01$  (approximately shorted), 50, and 100000 (approximately open) loads.

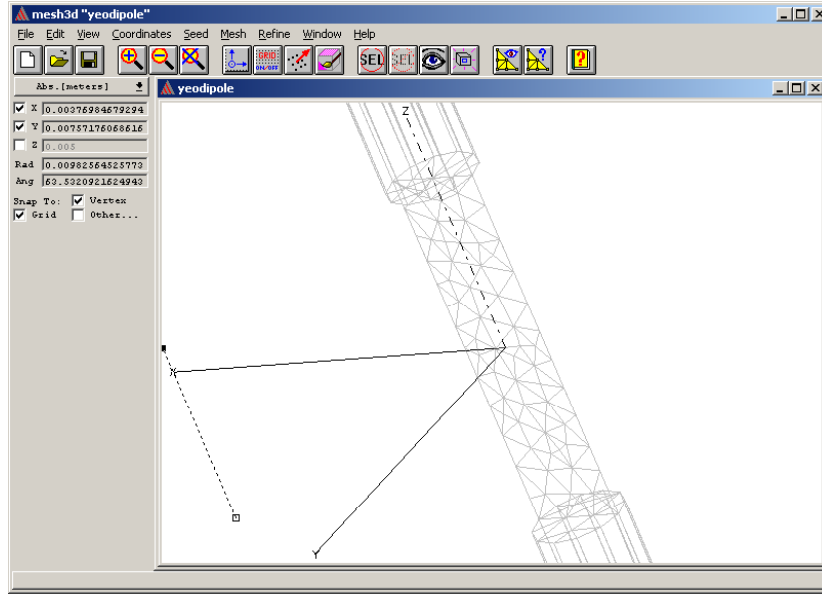


Figure 5: Rectangle in the dipole gap is meshed to compute electric field in the gap.

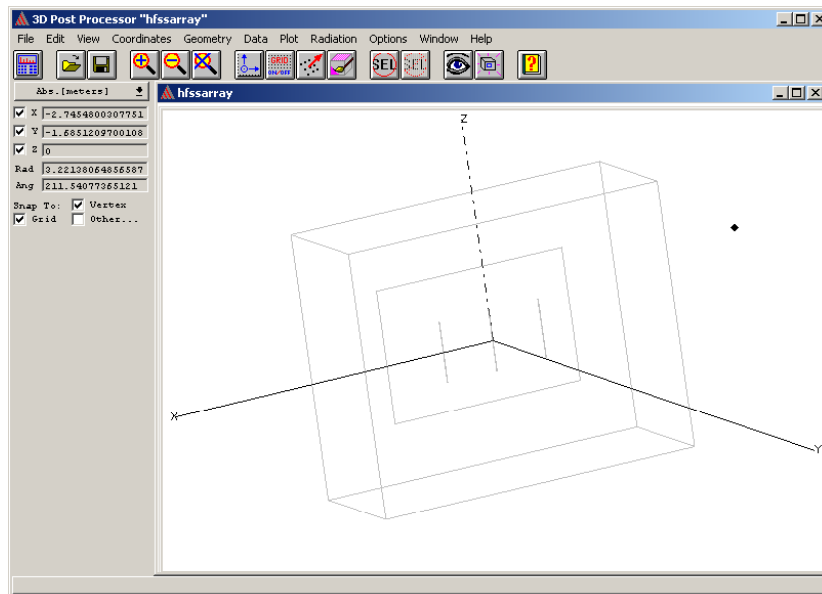


Figure 6: HFSS array model with radiation box.

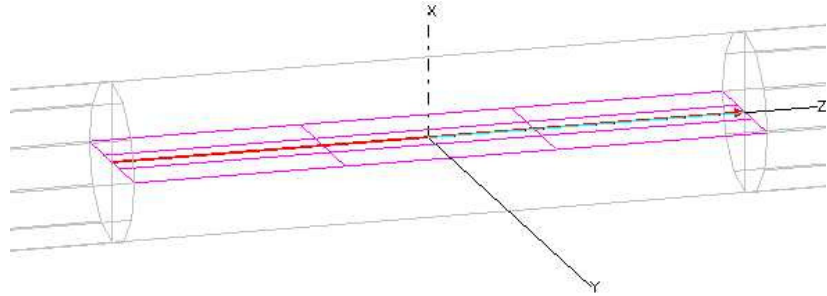


Figure 7: Two orthogonal rectangles in the gap. The lumped  $RLC$  boundary condition is assigned to one (highlighted) and a current source to the other.

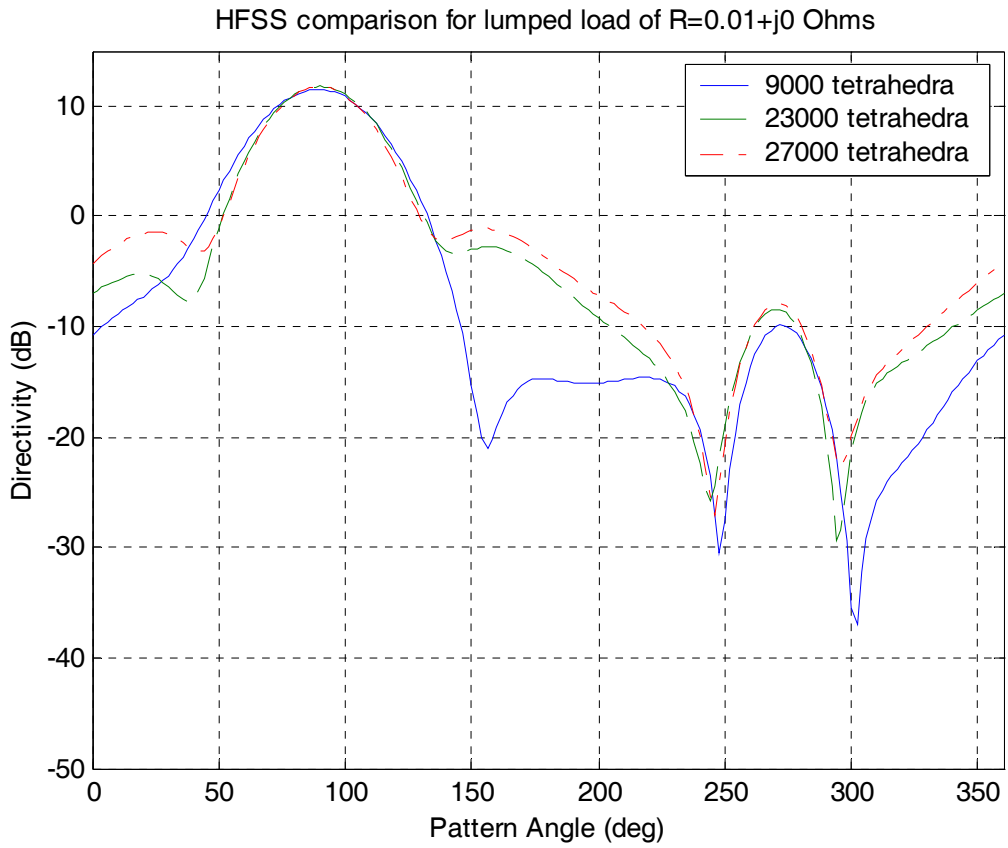


Figure 8: Patterns for various mesh densities.

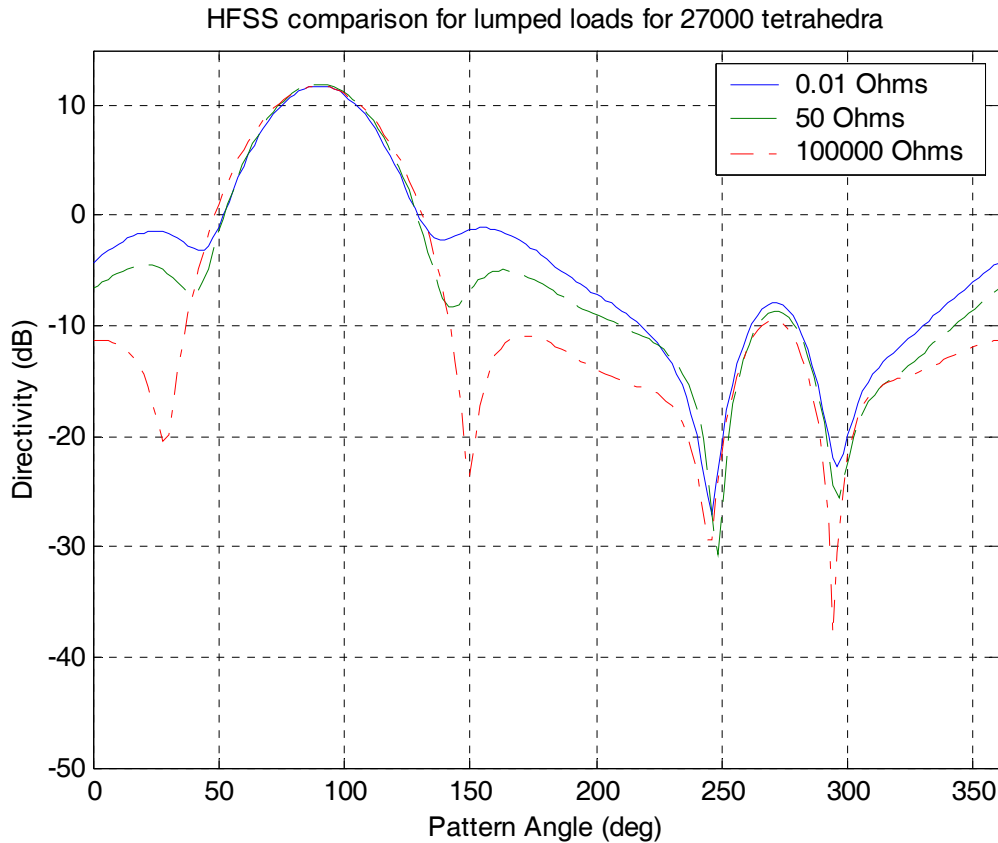


Figure 9: Radiation patterns for three load conditions.

### C. Finite Integration Technique

The finite integration technique (FIT) is a means of determining the radiated or scattered field from objects by solving Maxwell’s equations in integral form [7]. Update equations can be derived that give the field at a point in space and time as a function of the field at the same and neighboring points at previous times. Therefore the solution is said to “march in time.”

As with most numerical solutions, the computational region is discretized into appropriate subdomains. For receive or scattering problems, the incident wave is introduced into the computational grid and the fields computed throughout the grid as a function of time. The fields at the boundaries of the computational grid are used to compute equivalent currents, which, in turn, are used in the radiation integrals to compute the far field. The time domain fields can be Fourier transformed to obtain the frequency domain performance.

*Microwave Studio* by CST [8] is a FIT solver with a geometry builder and post processor. Rectangular meshing is used, but cells need not be filled with only one material. For ease of mesh control a dipole with a square cross section of 0.00125 m on a side was studied, as shown in Figure 10. As in the case of *HFSS*, a simple “Discrete Port” feed source is chosen even though *Microwave Studio* is capable of modeling a more complicated feed. The computational boundary was set about 0.15 m from the structure.

The fields can be plotted anywhere by setting up Monitors. Figure 11 shows a contour plot of the electric field in the region of the gap. The return loss (scattering parameters) and impedance (Figure 12) are computed automatically and available in the “1D Results” section. The impedance at 300 MHz was found to be  $53 - j 48$  ohms.

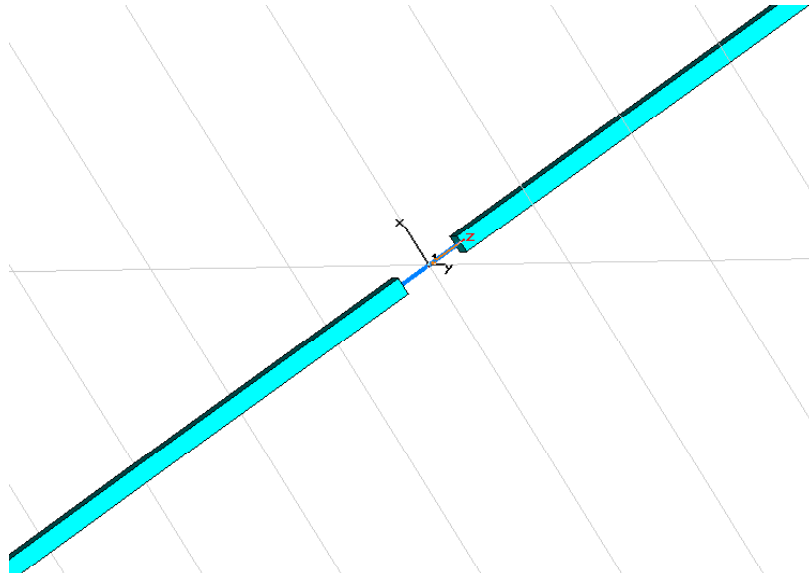


Figure 10: Square dipole model with a gap current source.

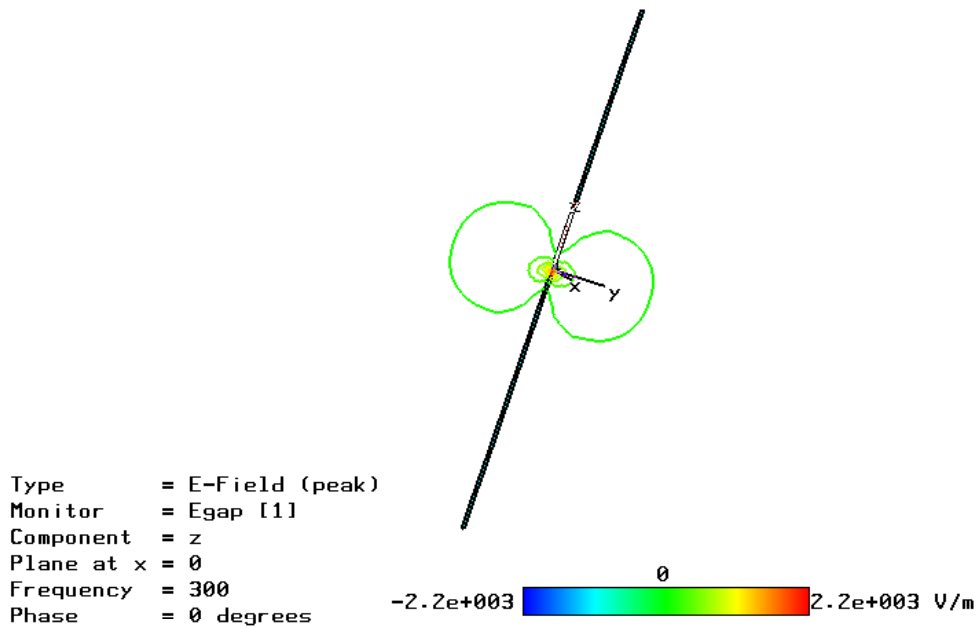


Figure 11: Contour plot of the field in the gap.

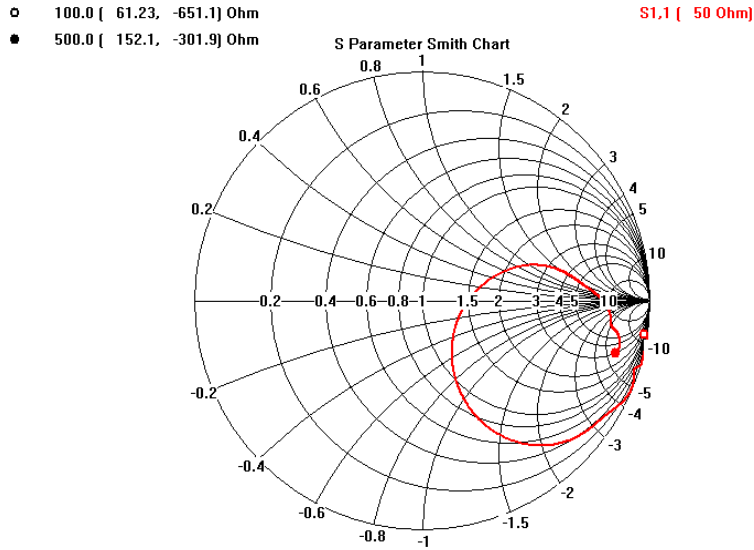


Figure 12: Dipole impedance computed from 100 MHz to 500 MHz.

The *Microwave Studio* array model is shown in Figure 13. The ground plane has a finite thickness of 0.01 m. The array patterns are shown in Figure 14 for three load conditions. A convergence level of -60 dB was requested for the solver, and the final number of meshnodes was about 800000.

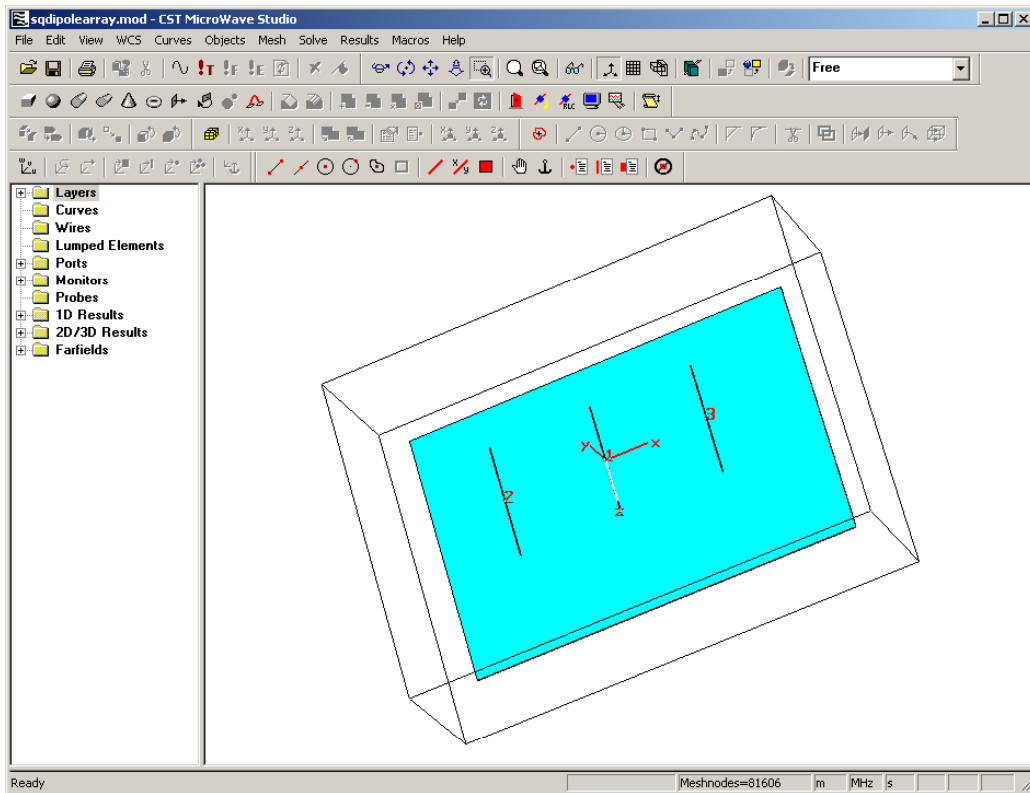


Figure 13: *Microwave Studio* model of the dipole array with ground plane showing the computational boundary.



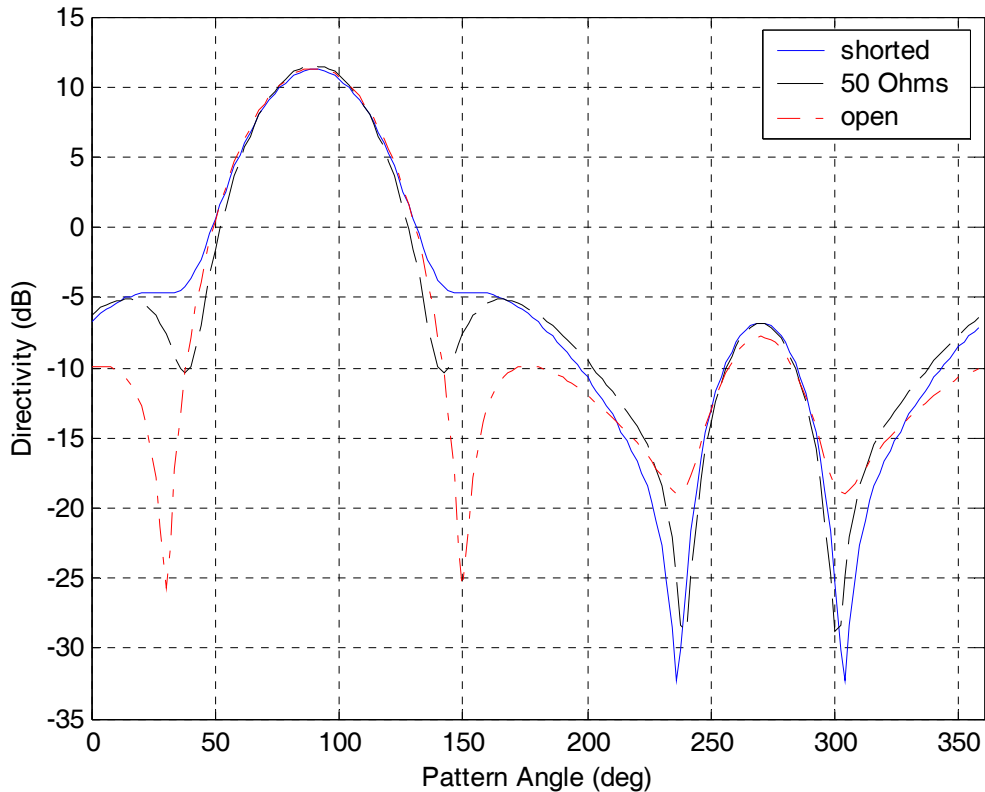


Figure 14: Comparison of directivity patterns for three load conditions.

#### D. Radar Cross Section

All three of the software packages are capable of solving antenna problems in the receive mode (plane wave incident) rather than the transmit mode. Also, electromagnetic scattering problems can be solved. Figure 15 shows the principal plane ( $\theta = 90^\circ$ ) bistatic RCS of a 3 wavelength square plate for a normally incident a plane wave. For each method, the plate is handled in a manner similar to the array ground plane: for MM it is infinitely thin and for FEM and FIT the ground plane thickness is 0.01 wavelength. The approximate number of subdomains in each case are: 2700 edges (MM), 55,000 tetrahedra (FEM) and 216,000 meshnodes (FIT).

#### E. Summary and Comments

Three popular numerical methods were used to solve some simple but fundamental radiation and scattering problems. Figures 15 and 16 summarize the results obtained using the three software packages. As expected, the agreement between the results was excellent when the structures are similarly modeled and the solutions converged. A “brute force” approach was used in setting up the models; no effort was made to try and optimize the computational efficiencies of the solutions. For example, in all three cases symmetry planes could be introduced to reduce the number of subdomains. Finite thickness ground planes could be replaced by infinitely thin surfaces with a PEC boundary condition applied. Also, there was no attempt to minimize the number of subdomains for a converged solution. Converged results could probably be obtained

with fewer subdomains in all cases. For these relatively small computational problems, there was no significant difference in the run times. The array calculations were in the range of 20 minutes on a 1.5 GHz PC, and all of the methods were within a couple of minutes of each other.

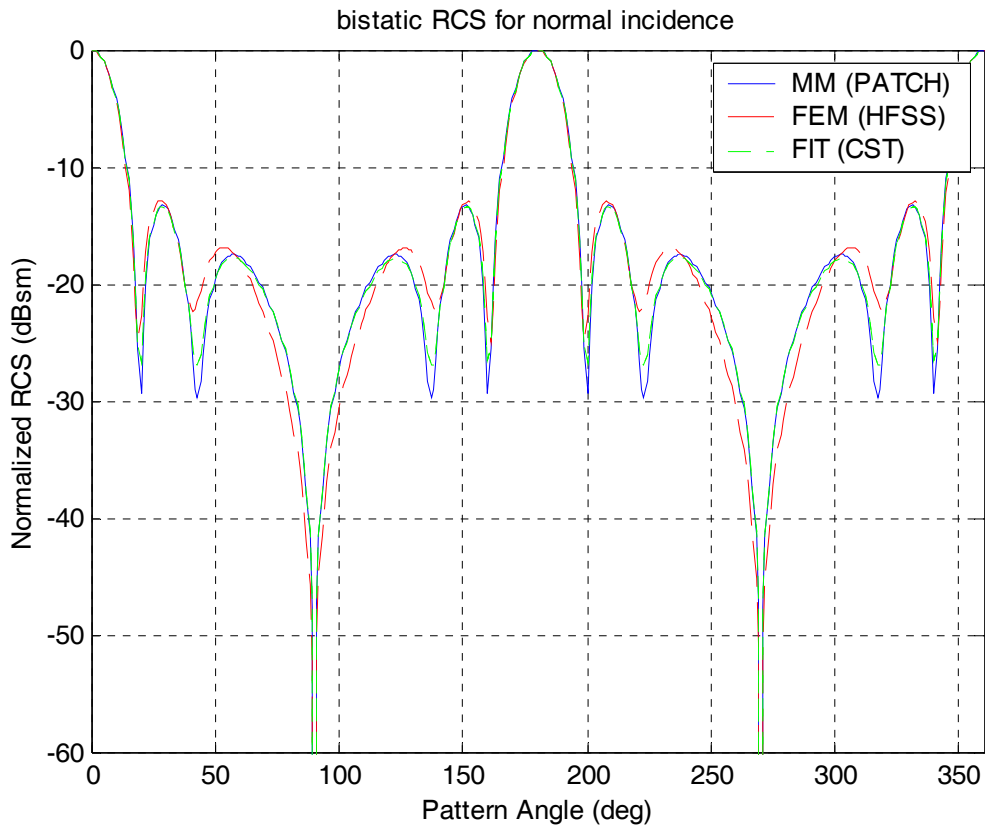


Figure 15: Bistatic RCS of a three-wavelength square plate.

## References

- [1] S. Rao, D. Wilton, and A. Glisson, "Electromagnetic Scattering by Surfaces of Arbitrary Shape," *IEEE Trans. on Antennas and Propagation*, vol. AP-30, no. 3, May 1982, pp. 409-418.
- [2] W. Johnson, D. Wilton, and R. Sharpe, *Patch Code Users' Manual*, Sandia Report SAND87-2991, May 1988.
- [3] E. A. Wolff, *Antenna Analysis*, Artech House, 1988.
- [4] Yeo Chee Beng, *Effects of Mutual Coupling in Small Dipole Array Antennas*, Naval Postgraduate School Master's Thesis, March 2002.
- [5] J. Volakis, A. Chatterjee and L. Kempel, *Finite Element Method for Electromagnetics*, IEEE Press, 1998.
- [6] [www.ansoft.com](http://www.ansoft.com)
- [7] M. Clemens and T. Weiland, "Discrete Electromagnetism with the Finite Integration Technique," *Journal of Electromagnetic Waves and Applications*, vol. 15, no. 1, 2001.
- [8] [www.cst.de](http://www.cst.de)

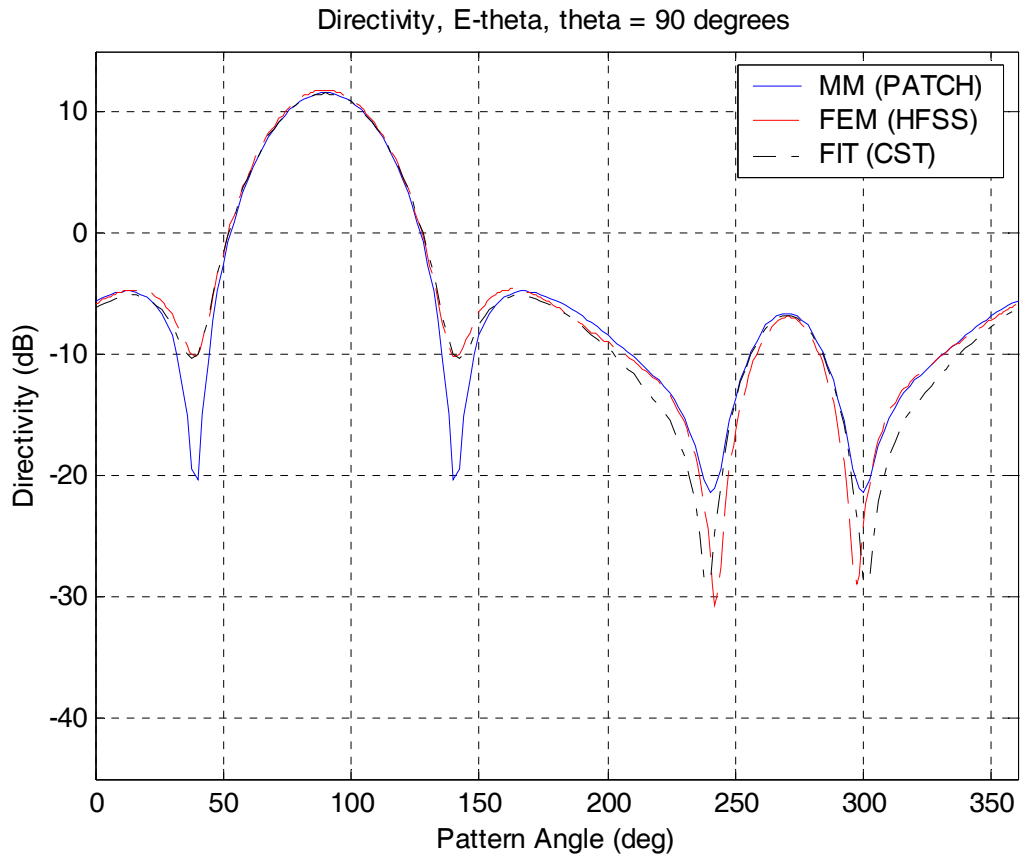


Figure 16: Overlay of the three radiation patterns for the dipole array, 50 ohm load.

# Two-Dimensional TM and TE FDTD Codes with Visualization

Allen W. Glisson<sup>1</sup>  
aglisson@olemiss.edu

Atef Z. Elsherbeni<sup>1</sup>  
atef@olemiss.edu

Chun-Wen P. Huang<sup>2</sup>  
cwhuang@anadigics.com

<sup>1</sup>Dept. of Electrical Engineering  
University of Mississippi  
University, MS 38677

<sup>2</sup>Anadigics, Inc.  
35 Technology Drive  
Warren, NJ 07059

## Introduction

This paper describes the use of two available two-dimensional Finite Difference Time Domain (FDTD) codes with visualization capabilities that have been developed primarily for educational use. The programs animate time domain scattering by a two-dimensional material geometry excited either by a  $z$ -directed electric current line source in the TM case (*tmpml*) or by a  $z$ -directed magnetic current line source in the TE case (*tepml*). A fairly general scattering geometry can be described by defining various regions with different isotropic constitutive parameters. The perfectly matched layer (PML) absorbing boundary condition is applied at the computational boundaries. The codes are available from the ACES web site <http://aces.olemiss.edu>.

## Code Components and System Requirements

The two programs and their associated example input data files comprise the following ten files:

tmpml.exe	tepml.exe
tmpml.dim	tepml.dim
tmpml.geo	tepml.geo
tmpml.vwc	tepml.vwc
tmpml.ind	tepml.ind

The codes were compiled with Compaq Visual Fortran version 6.6 and use the Compaq Array Viewer version 1.6. They have been tested under Windows 2000. In addition, if the machine on which the programs are to run does not have the Compaq Array Viewer installed, the user must obtain and install the Compaq Array Viewer Demo program. This “demo” is available on the web at

<http://www.compaq.com/fortran/>

If the user already has the Compaq Array Viewer installed, he should verify that the DLL file [aview160.dll](#) is in the Windows System directory.

## Program Usage

The programs *tmpml.exe* and *tepmml.exe* are “Fortran Console Applications” that run in a Command Prompt window. The user interacts with the FDTD program through keyboard input to the Command Prompt window. However, when so instructed by appropriate input data, the program invokes the Compaq Array Viewer for visualization of the solution. The Array Viewer program is a native Windows program. The user can interact with the Array Viewer program as with most Windows programs to change viewing angle, display method, plot parameters, etc.

The programs *tmpml.exe* and *tepmml.exe* can be run by any of the usual methods for executing Windows programs.

## Input Data Description

The descriptions of the input data files below are given explicitly for the TM program *tmpml.exe*. The data files for the TE program *tepmml.exe* are identical except that they begin with the letters “te” rather than “tm” and except for a few minor differences in the data definitions, which are identified in the descriptions when appropriate.

**Filename:** *tmpml.dim* — dynamic dimensioning parameters

Data required for dynamic dimensioning of the program arrays must be present in this data file in the form shown in Figure 1 (free format):

Ngx	Ngx
NPMLlayers	PMLpower
Nax	Nay

**Figure 1. Data format for the file *tmpml.dim*.**

Ngx and Ngx represent the numbers of “grid points” in the  $x$  and  $y$  dimensions of the computational grid in the TM case. These grid points are defined to be the points at which the

$z$  component of the electric field is computed. In the TE case,  $N_{gx}$  and  $N_{gy}$  represent the numbers of rectangular “cells” in the  $x$  and  $y$  dimensions of the computational grid. The center points of these rectangular cells are the points at which the  $z$  component of the magnetic field is computed in the TE case. All non-free-space materials of the scattering geometry reside within this computational grid. There is always one layer of free-space material surrounding the computational grid in addition to the PML region.  $N_{ax}$  and  $N_{ay}$  are the numbers of additional free-space layers to include between the computational grid and the PML region.  $NPMLlayers$  is the number of PML layers to be used to absorb the outgoing waves.  $PMLpower$  is the exponent in the expression for the rate of increase of  $\sigma$  as a function of distance from the air-PML interface within the PML region, typically 1, 2, 3, or 4.  $PMLpower$  is a real number; all other quantities in this file are integers.

**Filename:** *tmpml.vwc* — Array Viewer control parameters

Data required for initial control of the Array Viewer program must be present in this data file in the form shown in Figure 2 (free format):

```
IGeomDraw
IFieldDraw
IPlotStep
IPlotPause
PlotPeak
IFldComp
```

**Figure 2.** Data format for the file *tmpml.vwc*.

`IGeomDraw` controls whether or not the Array Viewer is used to display a schematic representation of the geometry before computation begins. A value of 1 turns geometry visualization on, and a value of 0 turns it off. `IFieldDraw` controls whether or not the Array Viewer is used to display the value of a field component during execution. A value of 1 turns field visualization on, and a value of 0 turns it off. If field visualization is on, the remaining values will control the initial visualization parameters.

`IPlotStep` controls the plot update frequency. If `IPlotStep` is set to a value of  $n$ , the field plot will be updated every  $n^{\text{th}}$  time step. The more often the field plot is updated, the slower the simulation will run. `IPlotPause` controls the number of time steps before execution is paused. If `IPlotPause` is set to a value of  $n$ , the simulation will be paused at every  $n^{\text{th}}$  time step. `IPlotPause` is useful to allow the user to interact with the FDTD program (instead of the Array Viewer program). When the FDTD program is paused in this manner, the user can take time to view the field plot more carefully, or can interact with the FDTD program to change the current values of `IPlotStep` and/or `IPlotPause`. To

interact with the FDTD program, or even to continue execution from the paused state, however, the Command Prompt window must be the “active window.”

The variable `PlotPeak` is used to set the maximum magnitudes of the field values to be displayed by the Array Viewer program.

The variable `IFldComp` is used to choose which field component is to be displayed. For the TM case the choices are 1 for  $E_z$ , 2 for  $H_x$ , or 3 for  $H_y$ . The peak value variable `PlotPeak` is then used to determine the peak value of  $E_z$  that would be displayed. If  $H_x$  or  $H_y$  is chosen for display instead, the value of `PlotPeak` is automatically adjusted by the free-space impedance value  $\eta_0$ . For the TE case the values of `IFldComp` for the various component choices are 1 for  $E_x$ , 2 for  $E_y$ , or 3 for  $H_z$ . The peak value variable `PlotPeak` in this case is used to determine the peak value of  $H_z$  that would be displayed. If  $E_x$  or  $E_y$  is chosen for display instead, the value of `PlotPeak` is automatically adjusted by  $\eta_0$ . `PlotPeak` is a real variable; all other variables in this file are integers.

**Filename:** *tmpml.geo* — scatterer geometry data

Data required to describe the scatterer geometry must be present in this data file in the form shown in Figure 3 (free format):

NumMatDefs				
MatID	epsr	mur	sigmae	sigmam
MatID	epsr	mur	sigmae	sigmam
:				
:				
:				
MatID	epsr	mur	sigmae	sigmam
ID	nxstart	nxend	nystart	nyend
ID	nxstart	nxend	nystart	nyend
:				
:				
:				
ID	nxstart	nxend	nystart	nyend
-1	0	0	0	0

**Figure 3.** Data format for the file *tmpml.geo*.

The first line of this data file identifies the number of different materials (`NumMatDefs`) to be defined to the program in subsequent lines of the data file. `NumMatDefs` must be between 1 and 50, allowing for use of 50 different materials as part of the scatterer geometry. Following the first line there must be `NumMatDefs` lines of data describing the materials. These subsequent data lines must specify the integer material identification number (`MatID`), the relative permittivity  $\epsilon_r$  (`epsr`), the relative permeability  $\mu_r$  (`mur`), the electric conductivity  $\sigma^e$  (`sigmae`), and the magnetic conductivity  $\sigma^m$  (`sigmam`). Thus, the first `NumMatDefs+1` lines of this data file represent material definition data available to the program. Note that these are just material definitions; it is not necessary for each material defined here to be used in the scatterer geometry to be simulated.

In addition to the definitions noted in the preceding paragraph, the free-space material type is predefined with a material ID of 0, while the perfect electric conductor (PEC) material type is predefined with a material ID of 51. These two material types can be used in the definition of the scatterer along with the other material types provided by the user. Any or all of the defined material types can be used in a particular scatterer geometry.

The user must define the scatterer geometry starting in line `NumMatDefs+2` of this data file. The geometry is defined in rectangular blocks by specifying a material ID (`ID`) and the range occupied by the material in the  $x$  and  $y$  dimensions in terms of the computational grid indices `nxstart`, `nxend`, `nystart`, and `nyend`. For the TM case, note that these quantities represent *node* or *grid point* values where the  $z$  component of the electric field is computed. Thus, in the TM case, the materials are specified to fill the spatial region with the corners defined by the four specified nodes. For the TE case, the quantities `nxstart`, `nxend`, `nystart`, and `nyend` represent *cell* number values where the  $z$  component of the magnetic field is computed. Thus, in the TE case, the materials are specified to fill the entire spatial region with the corners defined by the outermost corners of the four specified cells.

Each successive geometry specification line overwrites any material type previously specified for the indicated region. Thus, for example, one can create a hollow, rectangular dielectric cylinder by first creating a solid dielectric cylinder with the exterior dimensions desired, and then specifying the interior hollow region to have material ID 0. The interior region that was originally specified as dielectric material will be replaced with the new material type of free space.

Scatterer geometry input is terminated by specifying a material type of  $-1$  (negative one; the computation grid ranges must still be present as suggested by the data file form shown in Figure 3, but they are not used). When the material type of  $-1$  is encountered, no further data lines are read by the program.



**Filename:** *tmpml.ind* — other input data

Other input data required to describe the number of time steps to use, the spatial increments, the excitation, the saved field values, the output data file names, etc., must be present in this data file in the form shown in Figure 4 (free format):

The descriptions of the input variables in this file follow:

Nstop Final time step number to use.

JzAmp For the TM case this value represents the excitation electric current line source (Real, signed) amplitude. For the TE case this is instead MzAmp – the excitation magnetic current line source amplitude.

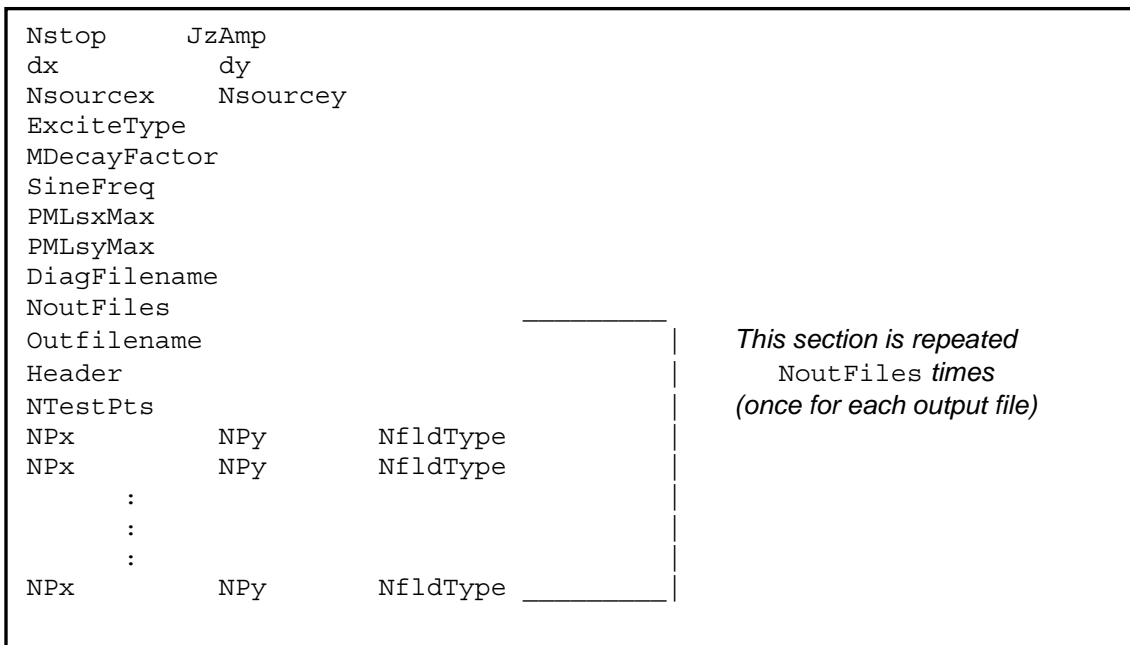


**Figure 4.** Data format for the file *tmpml.ind*.

dx, dy Spatial increment values (Real) in *x* and *y* in meters.

Nsourcecx,  
Nsourcecy For the TM case these values represent the *node* indices in the *x* and *y* directions within the computational grid of the electric current line source  $J_z$ . For the TE case they represent the *cell* indices in the *x* and *y* directions

within the computational grid of the magnetic current line source  $M_z$ . The magnetic current line source is located at the center of the specified cell.

**ExciteType** Excitation type (Character): there are two allowed current source excitation types that must be entered starting in column 1 *exactly* as shown in one of the following forms:

sine            A sine wave starting at  $t=0$   
 Gaussian      A Gaussian pulse

**MDecayFactor** Integer  $M$  that controls the decay rate of the Gaussian pulse. It is used to compute the inverse Gaussian decay constant  $\tau = M \max(\Delta x, \Delta y) / (2c\sqrt{3})$ . A value must appear in the data file for this variable in all cases, but is used only for the “Gaussian” excitation.  $M$  should be chosen such that  $M \approx \sqrt{3} n_c$ , where  $n_c$  is the number of cells to be used per wavelength at the maximum usable frequency.

**SineFreq** Sine wave frequency in GHz. A value must appear in the data file for this variable in all cases, but is used only for the “sine” excitation.

**PMLsxMax,**  
**PMLsyMax** The maximum values of the electric conductivity to be used in the PML region in the  $x$  and  $y$  directions.

**DiagFilename** The name (character\*16) of the diagnostic output file.

**NoutFiles** Number of output data files (maximum of 10).

**Outfilename** The name (character\*16) of the data output file.

**Header** The header string (character\*70) to appear in the data output files.

**NTestPts** The number of test points at which to save and print the field values (maximum of 500).

**NPx, NPy,**  
**NFldType** For the TM case  $NPx$  and  $NPy$  specify the *node* indices in the  $x$  and  $y$  directions within the computational grid at which the field value is to be saved for printing.  $NFldType$  specifies which field component to save: 1 for  $E_z$ , 2 for  $H_x$ , or 3 for  $H_y$ . For  $H_x$  and  $H_y$ , which are located between “nodes,” the value saved is the next value encountered in the

increasing index direction from the node (NPx, NPy). For  $H_y$ , for example, this will be the value of  $H_y$  at the point represented by (NPx+1/2, NPy). For the TE case NPx and NPy specify the *cell* indices in the x and y directions within the computational grid at which the field value is to be saved for printing. NfldType specifies which field component to save: 1 for  $E_x$ , 2 for  $E_y$ , or 3 for  $H_z$ . For  $E_x$  and  $E_y$ , which are located between “cells,” the value saved is the next value encountered in the increasing index direction from the center of cell (NPx, NPy). For  $E_y$ , for example, this will be the value of  $E_y$  at the point represented by (NPx+1/2, NPy).

## Code Execution

When the code begins execution, a Command Prompt window similar to that shown in Figure 5 will appear. If IGeomDraw has been set to a value of one in the data file *tmpml.vwc* (*tepml.vwc* for the TE case), the geometry view window will also appear (Figure 6) and will be the active window. In the geometry window in Figure 6 the material ID number is plotted as a function of  $x$  and  $y$ . The sample geometry shows a 3-sided PEC box (material ID 51) that is filled with a material medium (material ID 10), and the remainder of the space is filled with homogeneous free space (material ID 0).

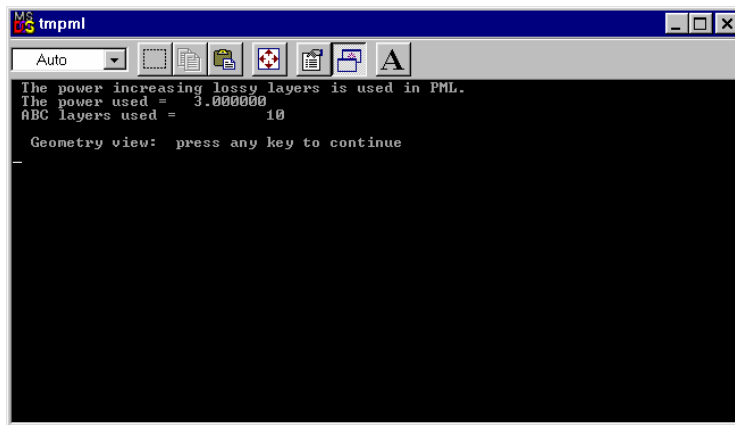
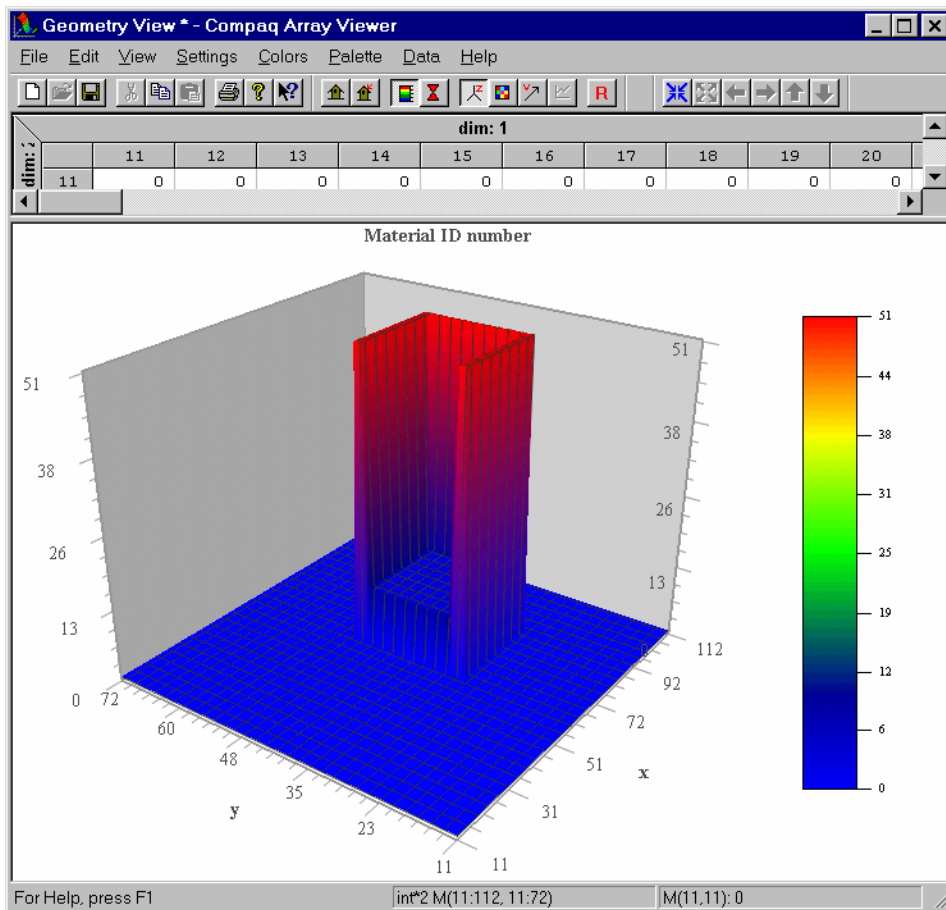


Figure 5. The *tmpml* Command Prompt window.

With the geometry window open, the user may rotate the schematic geometry view interactively with the mouse to obtain different views. The user may also interact with the menu items and tool bars of the Array Viewer program to zoom in to view a smaller region

of space (i.e., the material ID array), change the plot scale, change to an image map view of the array as shown in Figure 7, or change other Array Viewer options.



**Figure 6. The Array Viewer geometry view window of the program *tmpml* showing a 3D schematic representation of the geometry.**

One should note that the indexing scheme shown on the  $x$  and  $y$  axes includes the space required for the PML implementation. Thus, in the example above for which 10 PML layers were used, the indexing scheme begins with 11. The non-free space geometry, which was specified in the input data file to begin at node 50, shows up in the array as beginning at 61. By letting the mouse hover over a point in the image map of Figure 7 one can obtain quick (approximate) information on the particular array index and its value via a “tooltip-type” box, but the resolution is somewhat crude. Exact data can be obtained by using the array data window above the plot. The size of the data window can be increased as necessary.

To continue execution the user must first make the Command Prompt window the active window and then press any key to continue. The geometry view window will then

close and execution of the FDTD simulation will begin. Since the Command Prompt window must be the active window to continue execution after a pause, it may be convenient to reduce the font size of the Command Prompt window and allow it to remain as the top window once execution starts. Depending on the value of `IPlotPause` in the input data file `tmpml.vwc`, execution may continue until completion, or it may pause after a certain number of time steps. If execution pauses, the Command Prompt window will appear similar to that shown in Figure 8.

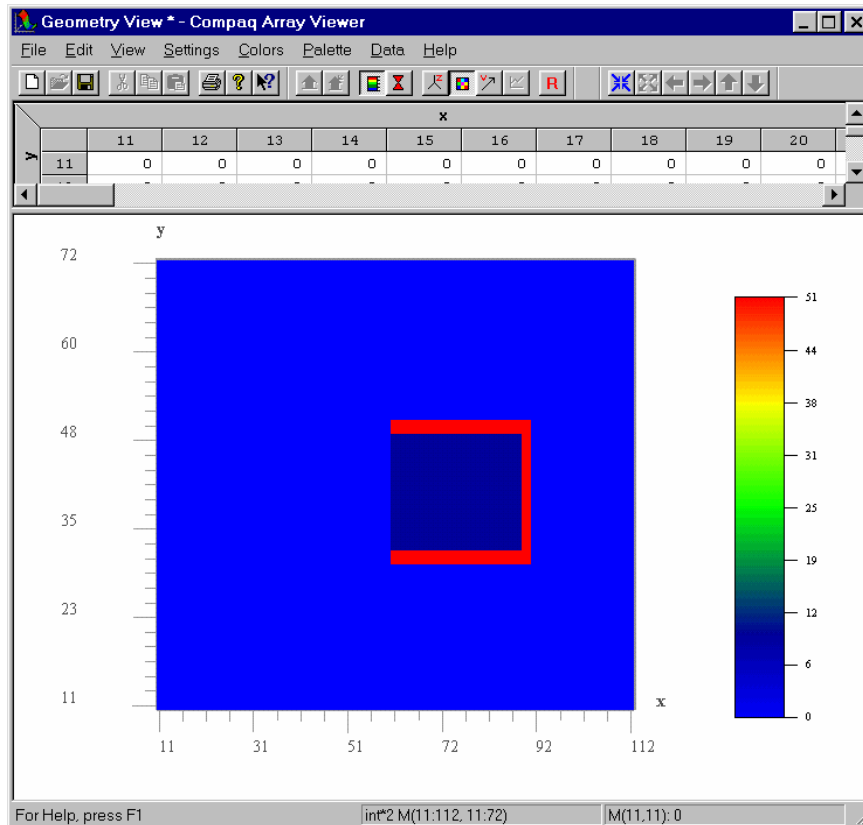


**Figure 7. The Array Viewer geometry view window of the program *tmpml* showing an image map schematic representation of the geometry.**

In the window shown in Figure 8 execution has been paused once at 100 time steps, then continued, and has been paused again at 200 time steps. While the program is in this paused state, if the user presses the “m” key a menu will appear as shown in Figure 9.

At this point the user can choose to abort the simulation immediately, to change the plot time spacing (i.e, change the current value of `IPlotStep`), or to change the pause time step spacing (change the current value of `IPlotPause`).

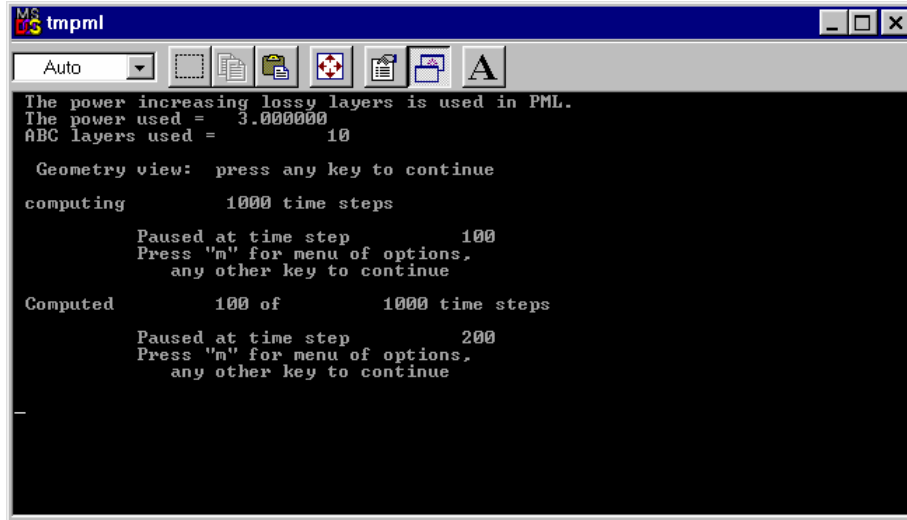


Figure 8. The *tmpml* Command Prompt window after execution has paused at a time step.

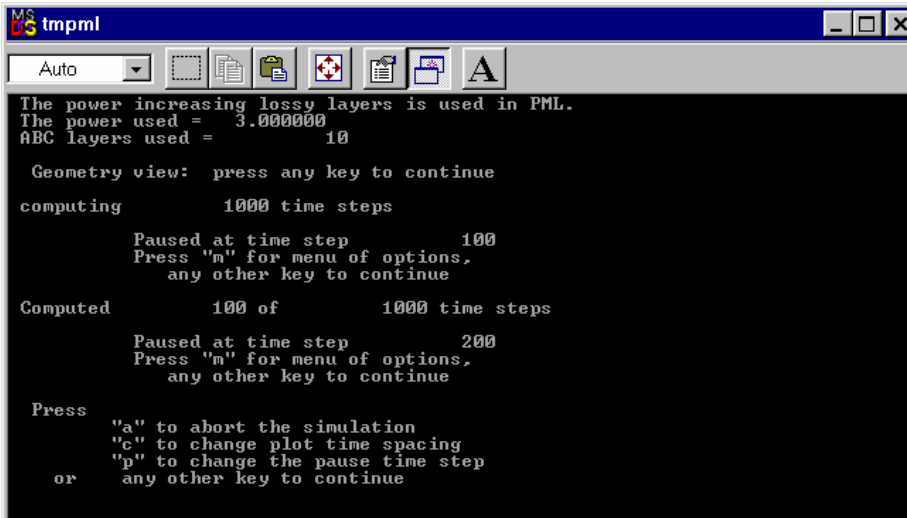
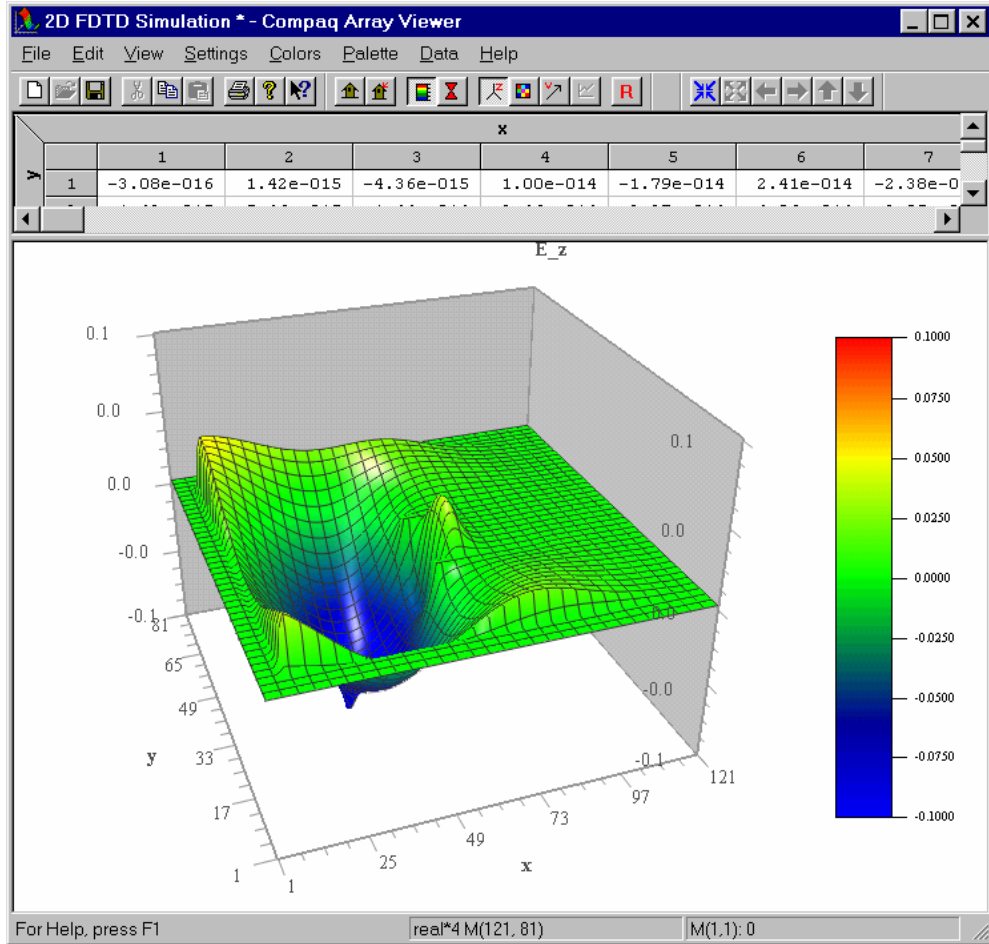


Figure 9. The *tmpml* Command Prompt window after the user has pressed "m" to get a menu of options.

For the TM case example data, when execution is paused at time step number 200 the Array Viewer window will appear similar to that shown in Figure 10. Note that the PML region surrounding the computational grid is also displayed in the simulation window.



**Figure 10. The Array Viewer simulation window of the program *tmpml* showing a 3D view of the electric field distribution.**

As with the geometry window, the user may rotate the view in the simulation window interactively with the mouse to obtain different views. The user may also interact with the menu items and tool bars of the Array Viewer program to zoom in to view a smaller region of space, change the plot scale, change to an image map view of the electric field distribution array as shown in Figure 11, or change other Array Viewer options.

The user can also find the current time step value and the current time value in picoseconds by using the Array View menu. To see this information select **Data**, then **Annotation...** The Annotation will appear as shown in Figure 12.

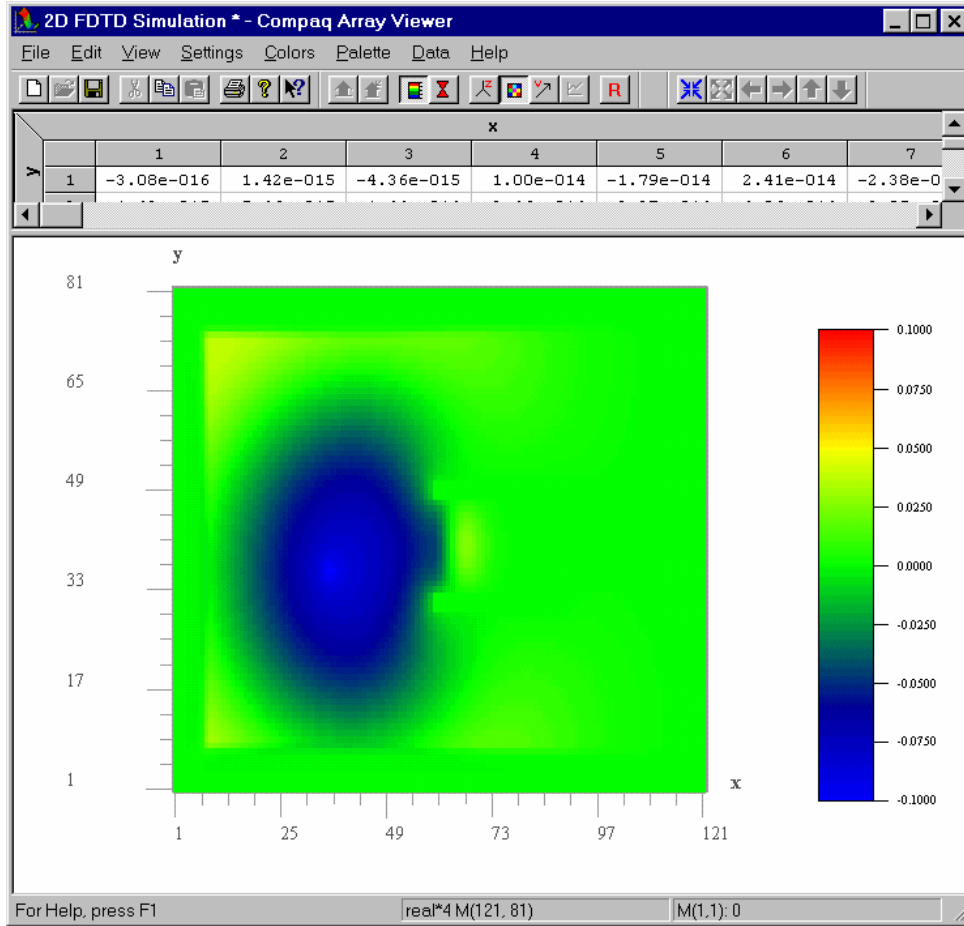


Figure 11. The Array Viewer simulation window of the program *tmpml* showing image map view of the electric field distribution.

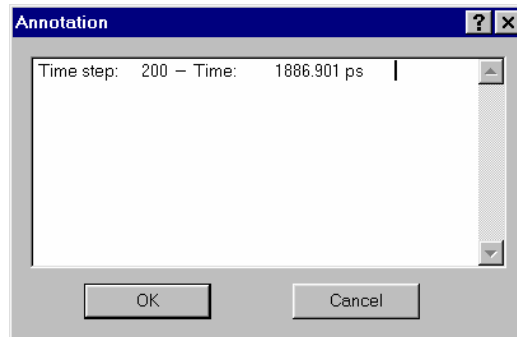
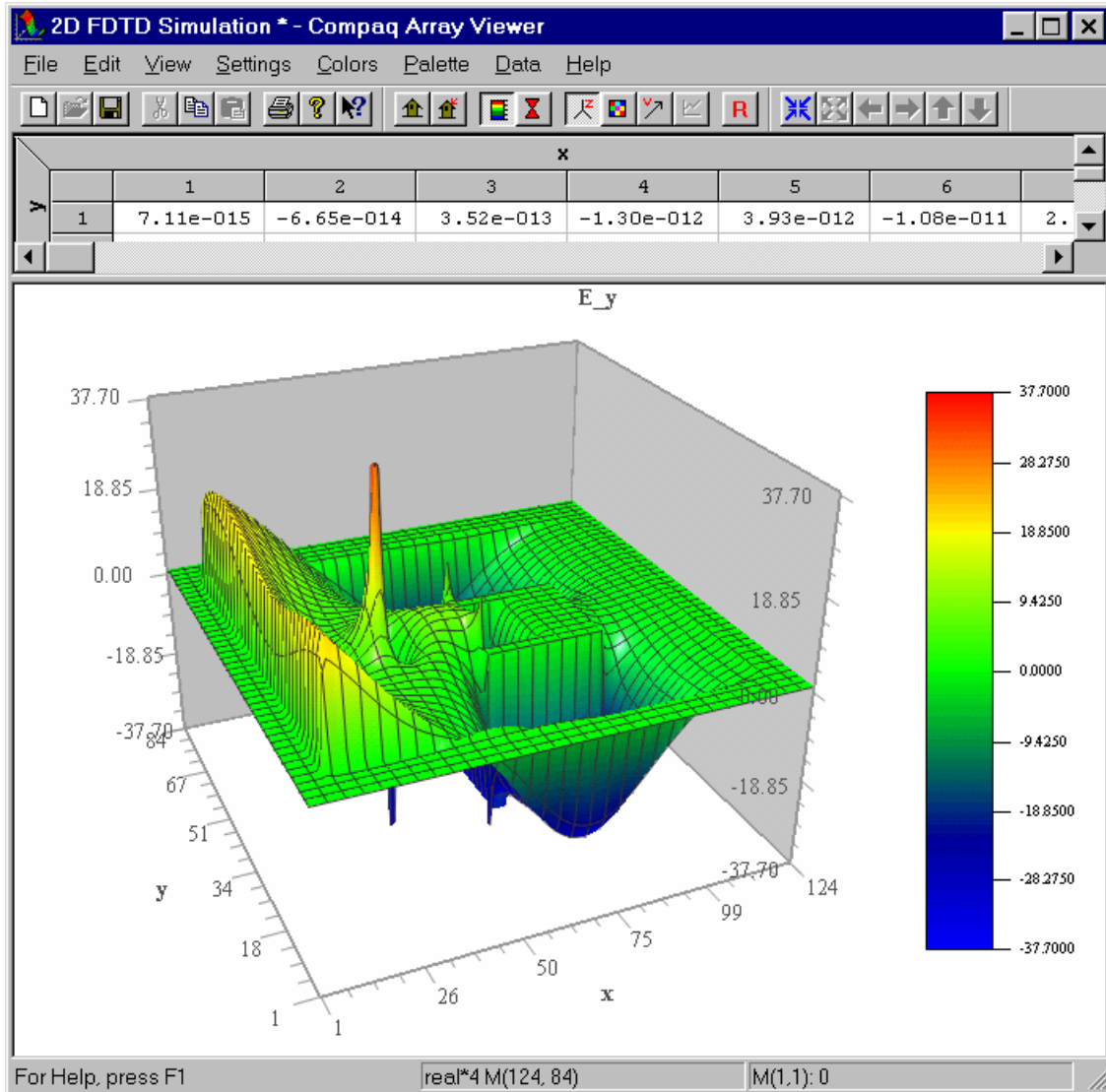


Figure 12. The Array Viewer Annotation window.



Execution of the TE program *tepm1.exe* proceeds in exactly the same manner. Example screens for the TE simulation case are shown in Figures 13 and 14, when execution is paused at time step number 200 for the sample data case.



**Figure 13.** The Array Viewer simulation window of the program *tepm1* showing a 3D view of the  $y$  component of the electric field distribution.

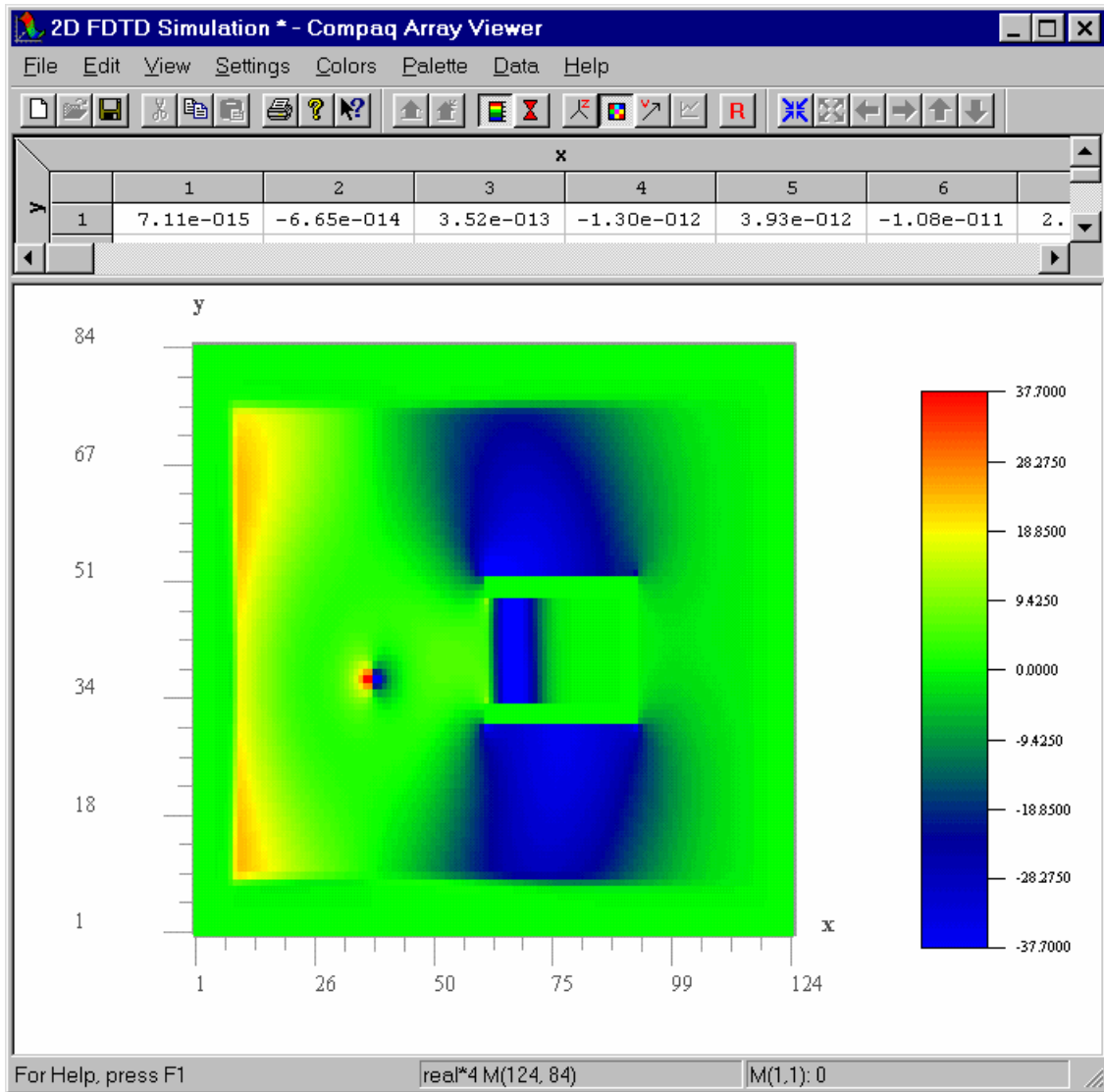


**Figure 14.** The Array Viewer simulation window of the program *tepm1* showing image map view of the *y* component of the electric field distribution.

**APPLIED COMPUTATIONAL ELECTROMAGNETICS SOCIETY**  
**RICHARD W. ADLER, EXECUTIVE OFFICER**  
**ECE DEPARTMENT, CODE ECAB, 833 DYER ROAD, ROOM 437**  
**NAVAL POSTGRADUATE SCHOOL, MONTEREY, CA 93943-5121,**  
**PHONE: 831-646-1111 FAX: 831-649-0300**  
**EMAIL: RWA@ATTGLOBAL.NET**

Please print

LAST NAME	FIRST NAME	MIDDLE INITIAL
COMPANY/ORGANIZATION/UNIVERSITY	DEPARTMENT / MAIL STATION	
MAILING ADDRESS WHERE PUBS MAY BE MAILED		
CITY	PROVINCE/STATE	COUNTRY
ZIP/POSTAL CODE		
TELEPHONE	FAX	AMATEUR RADIO CALL SIGN
E-MAIL ADDRESS		

	NEW MEMBERSHIP RATES (EFFECTIVE JANUARY 2003)			
	BASIC	INTERMEDIATE	EXPANDED	INSTITUTIONAL
WORLD AREA	Journal & Newsletter Access via Website & Annual (Nov) Searchable CD Rom of Proceedings of March Conference & Searchable CD ROM of year's Journals	BASIC, plus CD ROM of March Journal (Mar) & CD ROM of July Journal (Jul)	BASIC, plus Unbound Paper Copies of Journals (Mar, Jul, Nov)	BASIC, plus Bound Paper Copies of Journals (Mar, Jul, Nov)
US, CANADA and MEXICO	\$35. USD	\$55. USD	\$90. USD	\$125. USD
ALL OTHER AREAS	\$35. USD	\$55. USD	\$110. USD	\$125. USD

FULL-TIME STUDENT/RETIRED/UNEMPLOYED: BASIC RATE IS \$20.00 USD FOR ALL COUNTRIES

**Non-USA participants: Prices are in U.S. dollars. All currencies must be converted to U.S. dollars payable by banks with U.S. affiliates. (1) Bank Checks must have U.S. address of bank; Checks are payable to "ACES", (2) U.S./International Money Order drawn in U.S. funds, payable in U.S. \$\$, (3) Credit Cards: Visa, MasterCard, Amex and Discover.**

**CREDIT CARD USERS**

PRINT CARD HOLDER NAME: \_\_\_\_\_

CREDIT CARD HOLDER SIGNATURE: \_\_\_\_\_

CREDIT CARD HOLDER ADDRESS: \_\_\_\_\_

ADDRESS, CONT: \_\_\_\_\_

CREDIT CARD ACCOUNT #: \_\_\_\_\_

CARD EXP. DATE: \_\_\_\_\_

2003

## ADVERTISING RATES

	FEE	PRINTED SIZE
Full page	\$200.	7.5" x 10.0"
1/2 page	\$100.	7.5" x 4.7" or 3.5" x 10.0"
1/4 page	\$ 50	3.5" x 4.7"
<p>All ads must be camera ready copy.</p> <p>Ad deadlines are same as Newsletter copy deadlines.</p> <p>Place ads with Ray Perez, Newsletter Editor, Martin Marietta Astronautics, MS 58700, PO Box 179, Denver, CO 80201, USA. The editor reserves the right to reject ads.</p>		

## DEADLINE FOR THE SUBMISSION OF ARTICLES

Issue	Copy Deadline
March	January 13
July	May 25
November	September 25

For the **ACES NEWSLETTER** send copy to Bruce Archambeault in the following formats:

1. A PDF copy.
2. A MS Word (ver. 97 or higher) copy.
3. An Adobe PageMaker copy. If any software other than WORD has been used, contact the Managing Editor, Richard W. Adler **before** submitting a diskette, CD-R or electronic file.